Chemical Geology 466 (2017) 678–695

Contents lists available at ScienceDirect

Chemical Geology

journal homepage: www.elsevier.com/locate/chemgeo

Iron-controlled oxidative sulfur cycling recorded in the distribution and isotopic composition of sulfur species in glacially influenced fjord sediments of west Svalbard

Laura M. Wehrmann[a,*], Natascha Riedinger[b], Benjamin Brunner[c,d], Alexey Kamyshny Jr[c,e,f], Casey R.J. Hubert[c,g], Lisa C. Herbert[a], Volker Brüchert[c,h], Bo Barker Jørgensen[c,i], Timothy G. Ferdelman[c], Michael J. Formolo[c,1]

[a] School of Marine and Atmospheric Sciences, Stony Brook University, Stony Brook, NY 11794-5000, USA
[b] Boone Pickens School of Geology, Oklahoma State University, Stillwater, OK 74078-3031, USA
[c] Biogeochemistry Group, Max Planck Institute for Marine Microbiology, D-28359 Bremen, Germany
[d] Department of Geological Sciences, The University of Texas at El Paso, El Paso, TX 79968, USA
[e] Department of Geological & Environmental Sciences, The Faculty of Natural Sciences, Ben-Gurion University of the Negev, Beer Sheva, Israel
[f] Department of Geology and Earth Systems Science Interdisciplinary Center, University of Maryland, College Park, MD 20742, USA
[g] Department of Biological Sciences, University of Calgary, Calgary, AB T2N 1N4, Canada
[h] Department of Geological Sciences, Stockholm University, Stockholm SE-106 91, Sweden
[i] Center for Geomicrobiology, Department of Bioscience, Aarhus University, 8000 Aarhus C, Denmark

ARTICLE INFO

Keywords:
Sediment biogeochemistry
Oxidative sulfur cycling
Arctic fjords
Sulfur and oxygen isotopes
Iron geochemistry

ABSTRACT

This study investigates how glacially delivered reactive iron (oxyhydr)oxide and manganese oxide phases influence the biogeochemical cycling of sulfur in sediments of three Arctic fjords and how the biogeochemical signatures of these processes are preserved. Results reveal differences in the concentrations of dissolved iron and manganese in pore-waters and the concentration of solid-phase sulfur species within individual fjords and amongst the three fjords, likely controlled by the varying input of reactive iron (oxyhydr)oxides to the sediment. Broadly, the stations can be divided into three categories based on their biogeochemical signals. Stations in the first category, located in Smeerenburgfjorden, are characterized by relatively low concentrations of (easily) reducible particulate iron phases, increasing concentrations of iron monosulfides, pyrite, and elemental sulfur with depth, and low pore-water dissolved iron and manganese concentrations. Biogeochemical processes at these stations are primarily driven by organoclastic sulfate reduction, sulfur disproportionation and the subsequent reaction and sequestration of sulfide in the sediment as iron monosulfide and pyrite. Sulfur and oxygen isotope values of sulfate display progressive enrichment in heavy isotopes with depth at these stations. In contrast, concentrations of (easily) reducible particulate iron phases and pore-water dissolved iron (up to 850 μM) and manganese (up to 650 μM) are very high at stations of the second and third category, located in Kongsfjorden and Van Mijenfjorden, while iron monosulfide and pyrite contents are extremely low. The amount of pyrite and its isotope values in conjunction with organic sulfur compounds provide evidence for a detrital origin of a fraction of these sulfur compounds. At the Kongsfjorden and Van Mijenfjorden stations, oxidative pathways of the sedimentary sulfur cycle, controlled by the high availability of reducible particulate iron phases, play an important role, leading to the effective recycling of sulfide to sulfate through sulfur intermediates and concomitant resupply of the sulfate reservoir with ^{32}S. In both fjords, elemental sulfur was only detected at the outer fjord stations grouped into the third category. Our study provides a framework for interpreting the Fe-S-C geochemistry of similar continental shelf areas in modern settings and ultimately for identifying these environments in the rock record.

* Corresponding author.
E-mail addresses: laura.wehrmann@stonybrook.edu (L.M. Wehrmann), natascha.riedinger@okstate.edu (N. Riedinger), bbrunner@utep.edu (B. Brunner), chubert@ucalgary.ca (C.R.J. Hubert), lisa.herbert@stonybrook.edu (L.C. Herbert), volker.bruchert@geo.su.se (V. Brüchert), bo.barker@bios.au.dk (B.B. Jørgensen), tferdel@mpi-bremen.de (T.G. Ferdelman), michael.j.formolo@exxonmobil.com (M.J. Formolo).
[1] Present address: ExxonMobil Upstream Research Company, Spring, TX, 77, 389, USA.

http://dx.doi.org/10.1016/j.chemgeo.2017.06.013
Received 3 February 2017; Received in revised form 5 June 2017; Accepted 7 June 2017
Available online 09 June 2017

1. Introduction

Biogeochemical transformations of sulfur in marine sediments represent important components of the global sulfur cycle. These processes include the microbial reduction of sulfate coupled to the oxidation of organic matter and methane (e.g., Froelich et al., 1979; Jørgensen, 1982; Reeburgh, 1983; Hoehler et al., 1994; Valentine and Reeburgh, 2000), with organoclastic sulfate reduction as the dominant terminal electron accepting pathway in anoxic marine sediments (Jørgensen, 1982). Organoclastic sulfate reduction is the main vector of sulfur removal from the oceanic sulfate reservoir at present (Vairavamurthy et al., 1995; Bottrell and Newton, 2006). The reactions of sulfide species (hydrogen sulfide, H_2S; bisulfide, HS^-; sulfide, S^{2-} –here collectively referred to as sulfide) with pore-water ferrous iron (Fe^{2+}) and solid-phase iron (oxyhydr)oxides and the subsequent formation of iron monosulfide (FeS), elemental sulfur (S^0), and pyrite (FeS_2) transfer reduced sulfide into the solid-phase and eventually the geological record (e.g., Berner, 1970, 1984; Wilkin and Barnes, 1996; Rickard and Luther, 1997; Butler and Rickard, 2000; Schoonen, 2004). The formation and burial of pyrite represents an important pathway for the storage of reduced sulfur on geological time scales and, together with the burial of organic carbon, contributes to the maintenance of an oxidized surface on Earth (Berner, 1982, 1989; Berner and Raiswell, 1983; Hensen et al., 2003). Additionally, reduced sulfur is present in marine sediments in the form of organically bound sulfur, such as organic sulfur compounds (OSC; Sinninghe Damste and de Leeuw, 1990; Anderson and Pratt, 1995; Werne et al., 2004). These compounds form by sulfurization reactions with sediment organic matter, involving pore-water sulfide, intermediate sulfur species, such as polysulfides, or S^0 (see Sinninghe Damste et al., 1989; Sinninghe Damste and De Leeuw, 1990; Kohnen et al., 1989; Brüchert and Pratt, 1996; Werne et al., 2004, 2008; for review).

About 75–90% of sulfide produced during microbial sulfate reduction in continental shelf sediments undergoes re-oxidation, thus regulating pyrite burial in marine sediments (Jørgensen, 1982; Canfield, 1989; Jørgensen and Kasten, 2006). A variety of abiotic and biotic sulfide oxidation pathways involving different electron acceptors are known from oxic and anoxic marine environments (e.g., Jørgensen and Nelson, 2004). Sulfide can undergo abiotic oxidation via reaction with iron and manganese oxides (e.g., Aller et al., 1986; Aller, 2014). In bioturbated sediments, solid-phase iron monosulfide and pyrite can furthermore be oxidized via reaction with oxygen (Luther, 1987; Luther and Church, 1988; Moses and Herman, 1991; Morse, 1991), nitrate (mostly FeS), iron oxides or manganese oxides (Aller and Rude, 1988; Canfield et al., 1993; Schippers and Jørgensen, 2001, 2002; Schippers, 2004; Mortimer et al., 2001). Reaction products of these oxidative sulfur pathways are typically intermediate sulfur species, including polysulfides, elemental sulfur, thiosulfate, polythionates and sulfite (Jørgensen and Bak, 1991; Zopfi et al., 2004; Luther and Rickard, 2005; Jørgensen and Kasten, 2006; Kamyshny, 2009). These intermediate sulfur species can be further oxidized to sulfate by chemoautotrophic bacteria using oxygen, nitrate or metal oxides (e.g., Fuseler and Cypionka, 1995). In the absence of these oxidants, sulfur disproportionating bacteria can access intermediate sulfur species to form sulfate and sulfide (Bak and Cypionka, 1987; Krämer and Cypionka, 1989; Thamdrup et al., 1993; Finster et al., 1998).

In typical mid- to low-latitude continental shelf environments oxidative sulfur cycling is most efficient in the surface centimeters of the sediment where bioturbation provides ample oxidants for abiotic and biotic sulfur oxidation reactions (e.g., Canfield et al., 1993; Thamdrup et al., 1994). Below the surface layer, pore-water sulfide and solid-phase pyrite often accumulate in these sediments although reoxidation reactions likely continue to occur, albeit at lower rates than in surface sediments. The biogeochemical setting of sedimentary environments in some high latitude areas, especially glacially influenced fjords, may deviate from this general pattern. These systems are often characterized by very high detrital iron and manganese oxide accumulation rates (Wehrmann et al., 2014), reflecting the input of dissolved and particulate iron and manganese from glacial runoff to the fjords (e.g., Statham et al., 2008; Raiswell et al., 2006, 2008; Bhatia et al., 2013; Wadham et al., 2013; Hawkings et al., 2014; Hodson et al., 2016). This is accompanied by comparably low organic carbon input and by its dilution in the sediment due to high influx of glacially derived clastic material (Vandieken et al., 2006a; Wehrmann et al., 2014). Consequently, dissimilatory iron and manganese reduction play an important role in these environments, and pore-water iron and manganese concentrations are typically very high (Kostka et al., 1999; Vandieken et al., 2006a, 2006b; Wehrmann et al., 2014). Sulfide produced during organoclastic sulfate reduction may be rapidly recycled throughout the sediment with little evidence for the occurrence of this mineralization pathway in pore-water sulfide or sulfate concentration profiles (Brüchert et al., 2001; Wehrmann et al., 2014). This is similar to the iron-sulfur-carbon (Fe-S-C) dynamics previously described for Amazon shelf muds where ferric iron (Fe(III)) is regenerated by periodic massive resuspension of the sediment (Aller et al., 1986).

The existence of overlapping manganese, iron, and sulfur redox zones in Arctic sediments can establish a reductive-oxidative sulfur cycle that remains to a high degree hidden, a phenomenon that has been observed in sediments below the sulfate-methane transition (Holmkvist et al., 2011; Brunner et al., 2016), and in marine oxygen minimum zones (Canfield et al., 2010a), coined cryptic sulfur cycling. The question becomes how such sulfur cycling can be detected (i.e., what geochemical tracers are most sensitive), and how this cycle affects biogeochemical signatures that are preserved in the sediment record (i.e., what geochemical signatures are altered and preserved). In this study, we investigate the biogeochemical cycling of sulfur linked to the input of glacially delivered reactive iron and manganese oxide phases in the sediments of three Arctic fjords with focus on the partitioning of reduced sulfur compounds amongst the different solid-phase sulfur pools, the sulfur isotope compositions of these pools, and the sulfur and oxygen isotope records of sulfate preserved in the pore-waters. This integrated approach provides an opportunity to measure the instantaneous modern precursor sulfur species together with the final product that is preserved in the geological record. Establishing these links is necessary to more accurately interpret the sulfur geochemistry preserved through time.

2. Study area and sampling sites

The three fjords investigated in this study - Smeerenburgfjorden, Kongsfjorden, and Van Mijenfjorden - are located on the west coast of Spitsbergen, which is the largest island of the Svalbard Archipelago, located between 74° and 81°N in the northern Greenland Sea (Fig. 1a). Svalbard has an area of 61,000 km^2 of which more than half is covered by polythermal and cold-based glaciers with thicknesses of > 100 m (Hagen et al., 1993; König et al., 2014). Of the Svalbard glaciers that are larger than 1 km^2, < 20% terminate in tidewater (König et al., 2014). Many of the tidewater glaciers are characterized by extensive subglacial drainage systems, which deliver large amounts of suspended material directly into the adjacent fjord waters (e.g., Hagen et al., 1993; Hodgkins, 1997; Hodgkins et al., 2003; Rippin et al., 2003). The fjords are also influenced by glacial runoff from land-terminating glaciers which crosses proglacial plains (Hagen and Lefauconnier, 1995; Hodgkins et al., 2009; Wadham et al., 2007).

Western Spitsbergen fjords are influenced by Atlantic Water, Arctic waters and glacial meltwater (Cottier et al., 2005; Nilsen et al., 2008). The Atlantic Water is delivered by the Western Spitsbergen Current and by the Svalbard Branch flowing poleward along the continental slope and western Svalbard shelf, and along the northern Svalbard slope, respectively (Cottier et al., 2005; Manley, 1995; Ślubowska-Woldengen et al., 2007). Intrusion of Atlantic Water across the shelf and into the fjords begins rapidly in midsummer and initiates intense seasonal

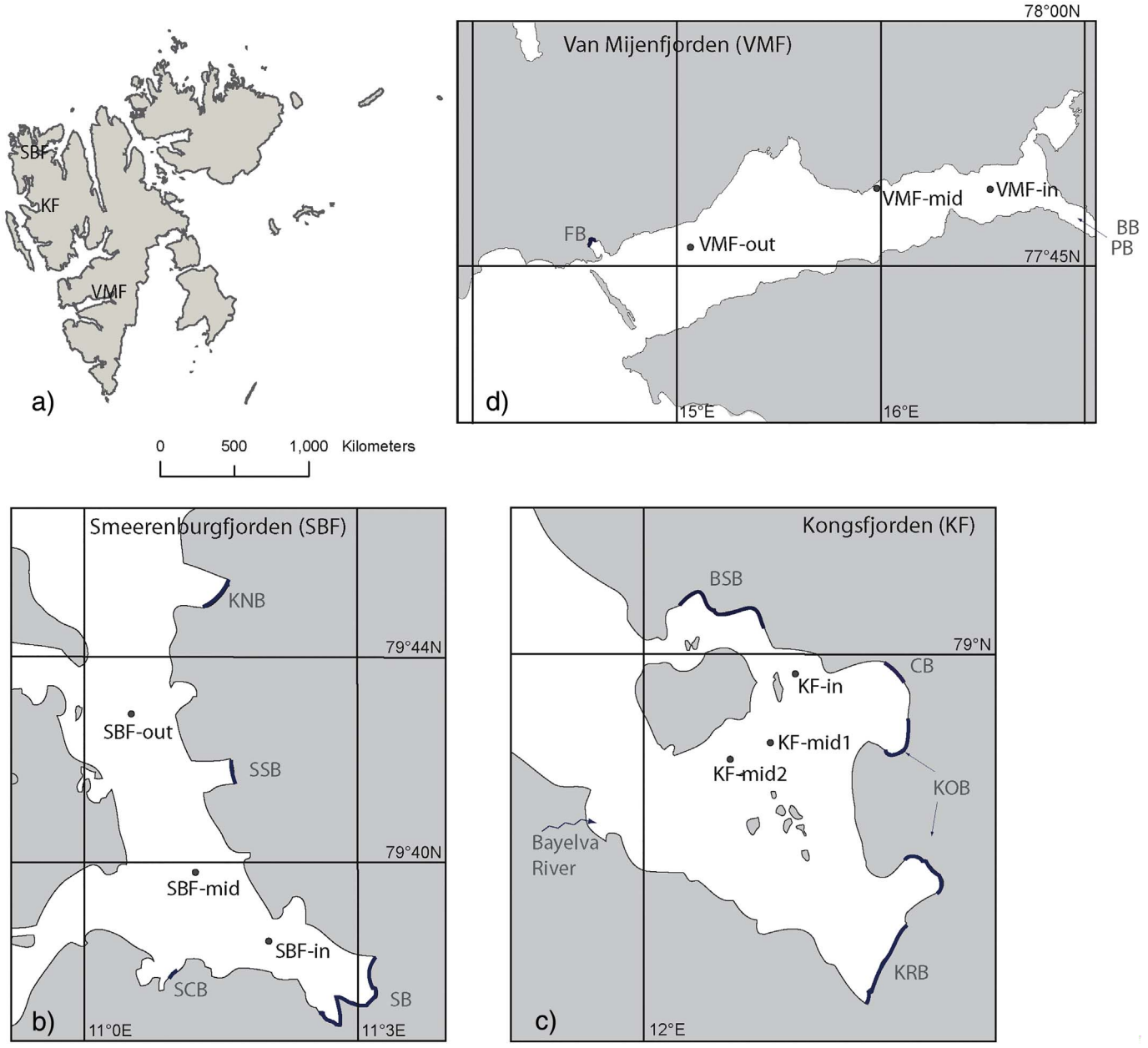

Fig. 1. a) Map of the Svalbard archipelago showing the locations of Smeerenburgfjorden (SBF), Kongsfjorden (KF), and Van Mijenfjorden (VMF). Detailed maps of the fjords and the sampling stations are presented in b) for Smeerenburgfjorden (Stations SBF-in, SBF-mid, and SBF-out) including the glacier-ocean interface (thick black line) of the tidewater glaciers Scheibreen (SCB), Smeerenburgbreen (SB), Kennedybreen (KNB), and Sellstrømbreen (SSB), c) for Kongsfjorden (Stations KF-in, KF-mid1, and KF-mid2) including the glacier-ocean interface of the tidewater glaciers Blomstrandbreen (BSB), Conwaybreen (CBR), Kongsbreen (KOB), and Kronebreen (KRB), and d) for Van Mijenfjorden (Stations VMF-in, VMF-mid, and VMF-out) including the glacier-ocean interface of the tidewater glaciers Fridtjovbreen (FB), Paulabreen (PB), and Bakaninbreen (BB).

variability of hydrographic conditions (Cottier et al., 2005). The influence of the Atlantic Water is responsible for essentially ice-free conditions west of the Svalbard shelf, the delivery of large amounts of nutrients by deep convection (Popova et al., 2010), and a relatively warm and variable climate as compared with other regions at the same latitude (König et al., 2014). Bottom water temperatures during the time of core collection are listed in Table 2. Commonly, the onset of the spring bloom in Kongsfjorden and other western Svalbard fjords is in May when ice cover starts to decrease (Eilertsen et al., 1989; Wiktor, 1999; Hop et al., 2002; Hegseth and Tverberg, 2013). However, in years when there is little or no ice, or ice-free periods, April blooms can occur depending on additional factors, particularly the inflow of Atlantic Water (Hodal et al., 2012; Hegseth and Tverberg, 2013).

The three investigated fjords, Smeerenburgfjorden, Kongsfjorden and Van Mijenfjorden display differences in the location and size of local glaciers that introduce meltwater, in total glacial coverage, and in bedrock composition of the catchment area (Table 1). Smeerenburgfjorden is a sound, open to the west and to the north, and its main glacier, Smeerenburgbreen, is a tidewater glacier located at the head of the fjord (Fig. 1b). The fjord is divided into three basins of up to 200 m water depth separated by large, often arcuate ridges. Sedimentation of fine-grained, meltwater-derived silts and clays has led to a smooth seafloor bathymetry in the outer basins. Holocene sediment thickness in the outermost basin is 10 m and increases fjord-inward to 20 m mid-fjord and 30 m in the innermost basin (Velle, 2012).

The most prominent tidewater glaciers entering Kongsfjorden are Kronebreen and Kongsvegen to the southeast and Blomstrandbreen to the north (Błaszczyk et al., 2009) (Fig. 1c). The fjord is also influenced by the Bayelva River, which provides glacial runoff to Kongsfjorden from the large land-terminating glacier Austre Brøggebreen to the

Table 1
Information on the three investigated fjords including length and width, and sizes of local glaciers (Błaszczyk et al., 2009; glacier area updated using the GLIMS Glacier Database), glacial coverage (Hagen et al., 1993; Svendsen et al., 2002), and bedrock composition (Steel and Worsley, 1984; Hjelle, 1993; Harland, 1997; Dallmann et al., 2002; Ohta et al., 2007; Ohta et al., 2008).

Fjord	Orientation	Length [km]	Width [km]	Glaciers	Total glacial catchment area and % glacial coverage	Bedrock composition
Smeerenburgfjorden	N-S, NNW-SSE	20	5	Smeerenburgbreen (109 km^2), Scheibreen (17 km^2); other glaciers < 12 km^2	232 km^2 (57%)	North and southwest: Granite, migmatite, banded gneiss (Mesoproterozoic Caledonian Smeerenburgfjorden Complex); Southeast and south: Hornemantoppen Granite
Kongsfjorden	E-W	22	12	Kongsbreen (379 km^2), Kronebreen (296 km^2), Kongsvegen (108 km^2), Infantfonna (78 km^2), Blomstandbreen (89 km^2), Sidevegen (65 km^2), Conwaybreen (54 km^2); other glaciers < 12 km^2	1100 km^2 (77%)	North: Mid-Proterozoic metamorphosed basement rocks including phyllite, schist, marble, bands of dolostone; South: Paleozoic sedimentary rocks, conglomerates, sandstones, carbonates, and spiculitic rocks; Locally, Tertiary rocks with conglomerates, sandstones, shales, and coal seams.
Van Mijenfjorden	E-W	83	10	Edvardbreen (61 km^2), Paulabreen (60 km^2), Fridtjovbreen (50 km^2), Bakaninbreen (56 km^2), Svalbreen (51 km^2), Scheelebreen (47 km^2), Slakbreen (36 km^2), Andrinebreen (29 km^2), Drønbreen (23 km^2), Vallåkrabreen (22 km^2), Kvitskarvbreen (20 km^2); other glaciers < 20 km^2	957 km^2 (37%; 66% in Rindersbukta)	Innermost part: Early Cretaceous sedimentary rocks; Remainder of the fjord: Palaeogene sedimentary bedrock of various types, including sandstones, siltstones, shales, coals and coal pebbles.

south, and by runoff from further glaciers on the southern coast, including Midre and Vestre Lovénbreen (Glasser and Hambrey, 2001). The fjord has an outer and a central basin of > 350 m water depth characterized by a smooth, flat seabed and an inner basin with a water depth of < 100 m (Howe et al., 2003). Holocene sediments in the outer and central basins have a thickness of < 10 m, while inner-fjord sediment cover is > 30 m thick (Howe et al., 2003).

Van Mijenfjorden is a large fjord that ends in two bays, Braganzavågen to the north and Rindersbukta to the south. Kjellströmdalen, a valley receiving glacial meltwater from several small glaciers debouches into Braganzavågen, while Rindersbukta receives direct input from three tidewater glaciers, Scheelebreen, Paulabreen and Bakaninbreen (Fig. 1d). Van Mijenfjorden has limited communication with the ocean because of an outer sill formed by the island Akseløya (Hald and Korsun, 2008). It can be divided into three basins with a maximum depth of 112 m at the outer basin, 74 m in the middle basin, and ~30 m in the inner basin (Hald and Korsun, 2008). The inner and middle basins are primarily filled with glaciogenic sediments with a thickness of > 30 m, while the outer basin is dominated by up to 20 m of glaciomarine sediments (Hald et al., 2001).

Several stations in Smeerenburgfjorden (SBF), Kongsfjorden (KF), and Van Mijenfjorden (VMF) were sampled in August 2008 aboard RV *Farm* (Fig. 1; Table 2). For simplicity, in this manuscript these stations are labeled according to their location within the fjords, e.g., SBF-in, SBF-mid, and SBF-out, for the inner, middle, and outer fjord stations at Smeerenburgfjorden, respectively. In the case of Kongsfjorden, there is a station proximal to the source of detrital input (KF-in), and two stations that are in the middle of the fjord (KF-mid1 and KF-mid2, Fig. 1c). The locations have been visited repeatedly during a longstanding research program (for example, Brüchert et al., 2001; Arnosti and Jørgensen, 2006; Robador et al., 2009; Canion et al., 2014) and have been reported using sampling station names that are different from the labels used in this study. A list of program station names together with our sampling site nomenclature can be found in Table 2.

3. Methods

3.1. Sample collection

Sediment cores were retrieved using a Haps corer (Ø 127 mm, 31.5 cm length; Kanneworff and Nicolaisen, 1983), except at SBF-out where a core was taken with a Rumohr corer (Ø 100 mm, 120 cm length; Mieschner and Rumohr, 1974). Cores were stored on deck (< 5 °C) until arrival at the Research Station in Ny Ålesund where the cores were subsampled. Bulk sediment samples were transferred into 50 mL centrifuge tubes with a depth resolution of 3 cm at all sites. Pore-water was extracted from the sediment by centrifugation and aliquots for pore-water sulfate and trace metal analyses were preserved with zinc chloride (10%, v/v) and trace metal grade nitric acid (1.5%, v/v), respectively. Sediment samples were subsequently stored in the dark at < 5 °C.

3.2. Solid-phase analyses

Sedimentary total carbon (TC) and nitrogen (TN) contents were determined with a Carlo Erba NA-1500 CNS analyzer on freeze-dried samples. Total inorganic carbon (TIC) was analyzed using a CM 5012 CO_2 coulometer (UIC) after acidification. The total organic carbon (TOC) content was calculated as the difference between TC and TIC. Analytical precision and accuracy determined by repeated analyses of an in-house standard DAN-1 for these analyses were better than 5%. The total organic carbon to nitrogen atomic ratio is displayed as C/N.

A four-step sequential extraction procedure was applied to freeze-dried sediment samples to target different operationally-defined iron mineral phases: Amorphous and nanoparticulate iron (oxyhydr)oxide phases (Fe_{ox1}) were extracted using an ascorbate solution (50 g L^{-1}

Table 2
Station name, sampling location, water depth, and bottom water temperature of the stations sampled in Smeerenburgfjorden, Kongsfjorden and Van Mijenfjorden.

Fjord	Station	Program station name	Location		Water depth [m]	Bottom water temperature [^{0}C]
Smeerenburgfjorden	SBF-in	GK	79°38,49 N	11°20,97E	175	1.9
	SBF-mid	GJ	79°39,75 N	11°12,82E	132	2.1
	SBF-out	J	79°42,83 N	11°05,10E	214	3.3
Kongsfjorden	KF-in	Q	78°59,43 N	12°17,87E	51	1.8
	KF-mid 1	P	78°57,87 N	12°15,14E	88	1.1
	KF-mid 2	R	78°57,42 N	12°09,66E	83	2.3
Van Mijenfjorden	VMF-in	AF	77°50,02 N	16°33,96E	67	− 0.8
	VMF-mid	GC	77°50,09 N	15°58,90E	31	2.7
	VMF-out	AH	77°45,82 N	15°03,82E	117	− 0.7

sodium citrate and 50 g L^{-1} sodium bicarbonate with 10 g L^{-1} of ascorbic acid added, pH 7.5, 24 h) following the procedure of Raiswell et al. (2008). Iron bound in carbonates was targeted with a sodium acetate solution (Fe_{carb}; 1 M sodium acetate buffered with acetic acid to pH 4.5; 48 h) and crystalline iron (oxyhydr)oxides (Fe_{ox2}) were extracted using a dithionite solution (50 g L^{-1} sodium dithionite buffered to pH 4.8 with acetic acid and sodium citrate; 2 h; Poulton and Canfield, 2005). Magnetite was extracted with an ammonium oxalate solution (Fe_{mag}; 0.2 M ammonium oxalate/0.17 M oxalic acid buffered with ammonium hydroxide to pH 3.2; 6 h; Poulton and Canfield, 2005). Extractions were done at room temperature by continuous shaking, and aliquots were taken after centrifugation (5000 rpm, 5 min). All solutions were freshly prepared prior to extraction, and reagent blanks were taken. The same extraction procedure was also applied to extract manganese phases from the freeze-dried sediment samples. Here, we present the sum of the concentrations determined by these steps as extractable manganese (Mn_{extr}). All extracts were analyzed by atomic absorption spectrometry (AAS) after 20-fold dilution. The ascorbate step likely extracts a fraction (< 30%) of the sedimentary iron monosulfide (AVS) pool (Kostka and Luther, 1994) and the subsequent sodium acetate step extracts the remainder of the AVS quantitatively (Poulton and Canfield, 2005). For the Smeerenburgfjorden stations, which contain significant concentrations of AVS in the sediment, Fe_{ox1} values thus slightly overestimate sedimentary amorphous and nanoparticulate iron (oxyhydr)oxide concentrations and the Fe_{carb} fraction is likely reflecting both carbonate-bound iron and AVS.

For elemental sulfur (S^0) concentration analysis a Sykam pump (S1100), a UV–Vis Detector (Sykam S3200), a Zorbax ODS-column (125 × 4 mm, 5 µm; Knauer, Germany), and 100% methanol (HPLC grade) at a flow rate of 1 mL per minute were employed following the method of Zopfi et al. (2004) using ~1 g of freeze-dried sediment (sample-to-extractant ratio ~1/10). Elemental sulfur was detected at 265 nm; the detection limit was about 1 µM, and the analytical precision of the method was ± 0.5% SD.

A two-step distillation method with cold 2 M HCl followed by a boiling 0.5 M $CrCl_2$ solution was applied to frozen sediment samples to determine the concentrations of AVS and chromium reducible sulfur (CRS) (FeS_2 and S^0; Fossing and Jørgensen, 1989). Concentrations of sulfide released during both distillation steps and trapped in zinc acetate were measured spectrophotometrically according to Cline (1969). Chromium reducible sulfur values were corrected for S^0 values determined in the methanol extraction and thus only represent FeS_2. The sediment remaining after Cr^{2+} distillation was triple washed with deionized water, filtered, and dried in a dessicator, and the sulfur content was analyzed with a Carlo Erba NA-1500 CNS analyzer. It is assumed to represent sulfur bound in organic matter (S_{org}) (Werne et al., 2003). A small fraction of this pool may also represent elemental sulfur (S^0; also analyzed in a separate extraction step; see above) as the Cr^{2+} distillation may not have quantitatively reduced all S^0, especially crystalline, rhombic elemental cyclooctasulfur (e.g., Fossing and Jørgensen, 1989; Gröger et al., 2009). However, the Cr^{2+} distillation likely extracted finely dispersed (and more prevalent) elemental sulfur formed in-situ in the sediment. We present the organic carbon to organic sulfur ratio as C/S. We plot C/S values against C/N values to explore whether trends in S_{org} concentrations within the three fjords are due to changes in the rate or pathways of sedimentary biogeochemical processes, or a function of dilution by lithogenic material.

3.3. Pore-water analyses

Sulfate concentrations were obtained after 100:1 dilution by non-suppressed anion exchange chromatography as described in Ferdelman et al. (1997) with IAPSO standard seawater (Canada) as reference standard. Chloride concentrations were not analyzed since samples were fixed with $ZnCl_2$. Analyses of pore-water dissolved iron (Fe_{diss}) and manganese (Mn_{diss}) concentrations were conducted on acidified pore-water aliquots after 10:1 dilution by inductively coupled plasma optical emission spectroscopy (ICP-OES; Leibniz Institute for Baltic Sea Research, Warnemünde) using CASS-4 as a reference standard. Precision (2σ) for ICP-OES was < 4% for all elements.

3.4. Isotope analyses

The stable sulfur isotope composition of pore-water sulfate, AVS, CRS, and S_{org}, is reported with respect to Vienna Canyon Diablo Troilite (VCDT) and the oxygen isotope composition of sulfate is reported with respect to Vienna Standard Mean Ocean Water (VSMOW) in the conventional delta notation. For the determination of the oxygen and sulfur isotope composition of sulfate, $ZnCl_2$-fixed aliquots were sonicated and filtered (0.45 µm) to remove ZnS. $BaCl_2$-solution (1 M, 0.3 mL) was added to HCl-acidified filtered samples to precipitate $BaSO_4$. Precipitates were washed several times with deionized water and dried. For isotope analysis of AVS and CRS, ZnS precipitates were converted to Ag_2S by treatment with 5% $AgNO_3$ and subsequently washed with 1 M NH_4OH to remove any colloidal silver. Sulfur isotope ratios were measured by weighing 0.4–0.6 mg of $BaSO_4$, 0.2–0.4 mg Ag_2S or 10–20 mg of S_{org} (residual material after chromium reduction; see Section 3.2) with an excess amount V_2O_5 into a tin capsule and combustion at 1060 °C in an elemental analyzer (EURO EA Elemental Analyzer) to produce SO_2. The evolved SO_2 was carried by a helium stream through a GC column, Finnigan Conflo III, and into a Finnigan Delta V stable isotope ratio mass spectrometer to determine $\delta^{34}S$. The sulfur isotope measurements were calibrated with reference materials NBS-127 ($\delta^{34}S = +21.1‰$) and IAEA-SO-6 ($\delta^{34}S = -34.1‰$). A silver sulfide laboratory standard ($\delta^{34}S = +4.8‰$, calibrated with AgS_2 standards) was repeatedly measured. In different measurement runs a $\delta^{34}S$ value of + 4.9‰ to + 5.1‰ was obtained. Consequently, an additional correction, i.e. the subtraction of 0.1‰ to 0.3‰ was performed on the AgS_2 samples. For oxygen isotope analyses, 0.3–0.4 mg of $BaSO_4$ was weighed into a silver capsule. The sample was carbothermically reduced at 1450 °C in a TC/EA (Thermo-Fisher) to yield carbon monoxide gas, which was analyzed in continuous flow mode with a Finnigan Delta V stable isotope mass spectrometer. The analytical reproducibility (σ1) of the isotope data based on repeated

measurements of laboratory standards was ± 0.2‰ for $\delta^{34}S$ and ± 0.8‰ for $\delta^{18}O$. The oxygen isotope measurements were calibrated with reference materials NBS-127 ($\delta^{18}O$ = 8.6‰), IAEA-SO-5 ($\delta^{18}O$ = 12.0‰) and IAEA-SO-6 ($\delta^{18}O$ = −11.3‰).

For triple sulfur isotope analyses, sulfur-containing samples were transformed to silver sulfide, which was converted to sulfur hexafluoride. Details of this procedure are reported in Zerkle et al. (2010). The isotopic abundance of the SF_6 was analyzed on a Finnigan MAT 253 dual inlet mass spectrometer at m/e- values of 127, 128, and 129 ($^{32}SF_5^+$, $^{33}SF_5^+$, $^{34}SF_5^+$, and $^{36}SF_5^+$). Typical standard deviations between analyses of $\delta^{34}S$ and $\Delta^{33}S$ were 0.02–0.05‰, 0.01–0.02‰, respectively. Long-term reproducibility for lab standards are 0.14‰ for $\delta^{34}S$ and 0.008‰ for $\Delta^{33}S$. Isotopic measurements are reported on a VCDT scale, assuming the composition of IAEA S-1 is $\delta^{34}S$ = −0.30‰ and $\Delta^{33}S$ = 0.094‰:

$$\Delta^{33}S = (^{33}R_{sample}/^{33}R_{VCDT}) - (^{34}R_{sample}/^{34}R_{VCDT})^{0.515} \quad (1)$$

where $^{3X}R_{sample}$ is the isotopic ratio of a sample:

$$^{3X}R = {}^{3X}S/{}^{32}S \text{ (for 3X = 33 or 34)} \quad (2)$$

and $^{3X}R_{VCDT}$ is the isotopic ratio of the starting sulfide relative to VCDT.

4. Results

4.1. Solid-phase composition

The sedimentary carbon and nitrogen contents reveal distinct differences between the three fjords. Sedimentary TOC contents ranged from 0.85 wt% at SBF-in to 1.60 wt% at SBF-out in Smeerenburgfjorden, from 0.48 wt% at KF-in to 0.82 wt% at KF-mid2 in Kongsfjorden, and from 2.07 wt% at VMF-in to 1.88 wt% at VMF-mid in Van Mijenfjorden (Table 3). Sedimentary TIC concentrations generally increased fjord-outward in all fjords with average values of 0.34–0.55 wt% in Smeerenburgfjorden, 1.26–2.23 wt% in Kongsfjorden, and 0.01–0.07 wt% in Van Mijenfjorden. Molar C/N ratios of sediment were ~9 in Smeerenburgfjorden, 19–22 in Kongsfjorden, and 15–20 in Van Mijenfjorden (Table 3).

Contents of iron extracted in the Fe_{ox1} fraction were 0.11–0.22 wt% at SBF-in and SBF-mid, and more variable with values of 0.03–0.28 wt% at SBF-out (Fig. 2a). All Kongsfjorden sites displayed Fe_{ox1} values of 0.08–0.13 wt% with little depth variation (Fig. 2e). Van Mijenfjorden stations were characterized by slightly higher Fe_{ox1} values, especially in the surface sediment, of up to 0.45 wt% (Fig. 2e, i). Variations in carbonate-bound Fe (Fe_{carb}) values of fjord sediments were more pronounced between the fjords with values < 0.16 wt% in Smeerenburgfjorden, ~0.6 wt% in Kongsfjorden, and 0.75–1.39 wt% in Van Mijenfjorden (Fig. 2b, f, j). Generally, at all stations Fe_{carb} values remained almost constant with depth. Large differences between the fjords were observed in sedimentary Fe_{ox2} contents. Smeerenburgfjorden sediments had Fe_{ox2} contents of 0.10–0.16 wt%, Kongsfjorden 0.61–1.08 wt%, and Van Mijenfjorden 1.24–2.07 wt% (Fig. 2c, g, k). Magnetite concentrations (Fe_{mag}) of Smeerenburgfjorden sediments were uniformly low at ~0.15 wt% (Fig. 2d). In Kongsfjorden, Fe_{mag} values were in the range of 0.54–0.94 wt% with no clear differences between the stations (Fig. 2h). Fe_{mag} values in Van Mijenfjorden were elevated at VMF-in (0.68–1.04 wt%) compared to VMF-mid which had contents of ~0.12 wt% (Fig. 2l).

Solid-phase Mn_{extr} contents ranged from values < 0.015 wt% in Smeerenburgfjorden (Fig. 3a), to 0.01–0.07 wt% in Kongsfjorden (Fig. 3b), and 0.01–0.64 wt% in Van Mijenfjorden. At the Van Mijenfjorden stations values were highest in the topmost 4 cm and decreased to values ~0.02 wt% in the deepest sections of the cores (Fig. 3c).

Contents of AVS in sediments of Station SBF-in showed little variation with depth, while at SBF-mid and SBF-out AVS increased with depth with a maximum value of 0.6 wt% observed in the deepest section of the SBF-out core (Fig. 4a). In contrast, AVS values at all Kongsfjorden and Van Mijenfjorden stations were below 0.03 wt% (Fig. 4e, i) with only subtle increases with depth. Similarly, solid-phase CRS concentrations at all Smeerenburgfjorden stations showed pronounced increases with depth; at SBF-out, CRS values reached 0.67 wt% (Fig. 4b). CRS concentrations ranged from 0.01 to 0.05 wt% at all Kongsfjorden and Van Mijenfjorden stations (Fig. 4f, i).

Elemental sulfur concentrations in Smeerenburgfjorden sediments increased with depth at all stations. SBF-out S^0 values reached 0.15 wt% in the deepest section analyzed (Fig. 4c). At the other fjords, increased S^0 values were only detected at KF-mid2 (maximum value 0.024 wt%) in Kongsfjorden and VMF-out (maximum value 0.032 wt%) in Van Mijenfjorden (Fig. 4g, k), while values were below 0.0025 wt% at all other stations.

At all stations S_{org} contents showed little variation with depth. Average S_{org} contents in Smeerenburgfjorden sediments increased seaward from values of ~0.015 wt% at SBF-in to values of ~0.03 wt% at SBF-out (Fig. 4d). At all Kongsfjorden stations, S_{org} values were < 0.01 wt% (Fig. 4h). At all Van Mijenfjorden stations sedimentary S_{org} values were in the range of 0.021–0.025 wt% (Fig. 4j). Molar C/S ratios were in a range of 125–175 at the Smeerenburgfjorden stations, 190–270 at the Van Mijenfjorden stations, and exhibited a more scattered distribution at the Kongsfjorden stations of 340–620 (Fig. 5).

4.2. Pore-water composition

The sulfate concentration measurements for all stations scattered over a wide range, with values that greatly exceeded the sulfate concentration of seawater (data not shown). These fluctuations are not mirrored in the sulfate isotope composition trends, and are not compatible with sulfate concentration profiles from stations that have been sampled during other campaigns. For example, Wehrmann et al. (2014) analyzed pore-water sulfate concentrations with depth at two stations in Kongsfjorden, including KF-in, and three stations in Smeerenburgfjorden, including SBF-in and SBF-out. The study displayed sulfate profiles for Kongsfjorden sediments that reflect typical marine values of ~28.2 mM with < 1 mM variation with depth, and profiles for the Smeerenburgfjorden stations that showed pronounced, continuous decreases with depth from typical seawater values at the sediment-water interface to values ~24 mM below 25 cmbsf at SBF-out (see Fig. S1a). Results from a previous analysis of pore-waters from Van Mijenfjorden VMF-out displayed sulfate concentrations of ~28.3 mM with < 0.5 mM variation in the topmost 30 cm of the sediment (Fig. S1c). Sulfate concentration analyses of cores retrieved during a sampling campaign in Summer 2016 also displayed < 1 mM variation in the top 30 cmbsf at stations KF-mid1 and VMF-in (Fig. S1b, c). This leads us to conclude that either sampling or measuring artifacts

Table 3
Total organic carbon (TOC), total inorganic carbon (TIC), total nitrogen (TN), organic carbon to nitrogen ratios (C/N ratios), and organic carbon to organic sulfur (C/S ratio; S_{org} determined on residue of two-step AVS-CRS distillation method) at the stations sampled in Smeerenburgfjorden, Kongsfjorden and Van Mijenfjorden (mean values for the top 20 cm).

Fjord	Station	TOC [wt%]	TIC [wt %]	TN [wt %]	C/N ratio [mol/mol]	C/S ratio [mol/mol]
Smeerenburgfjorden	SBF-in	0.85	0.34	0.11	9	157
	SBF-mid	1.09	0.44	0.14	9	151
	SBF-out	1.60	0.55	0.20	9	143
Kongsfjorden	KF-in	0.48	1.26	0.03	19	545
	KF-mid 1	0.62	2.08	0.04	19	442
	KF-mid 2	0.82	2.23	0.04	22	403
Van Mijenfjorden	VMF-in	2.07	0.01	0.12	20	256
	VMF-mid	1.85	0.01	0.12	18	213
	VMF-out	1.88	0.07	0.15	15	209

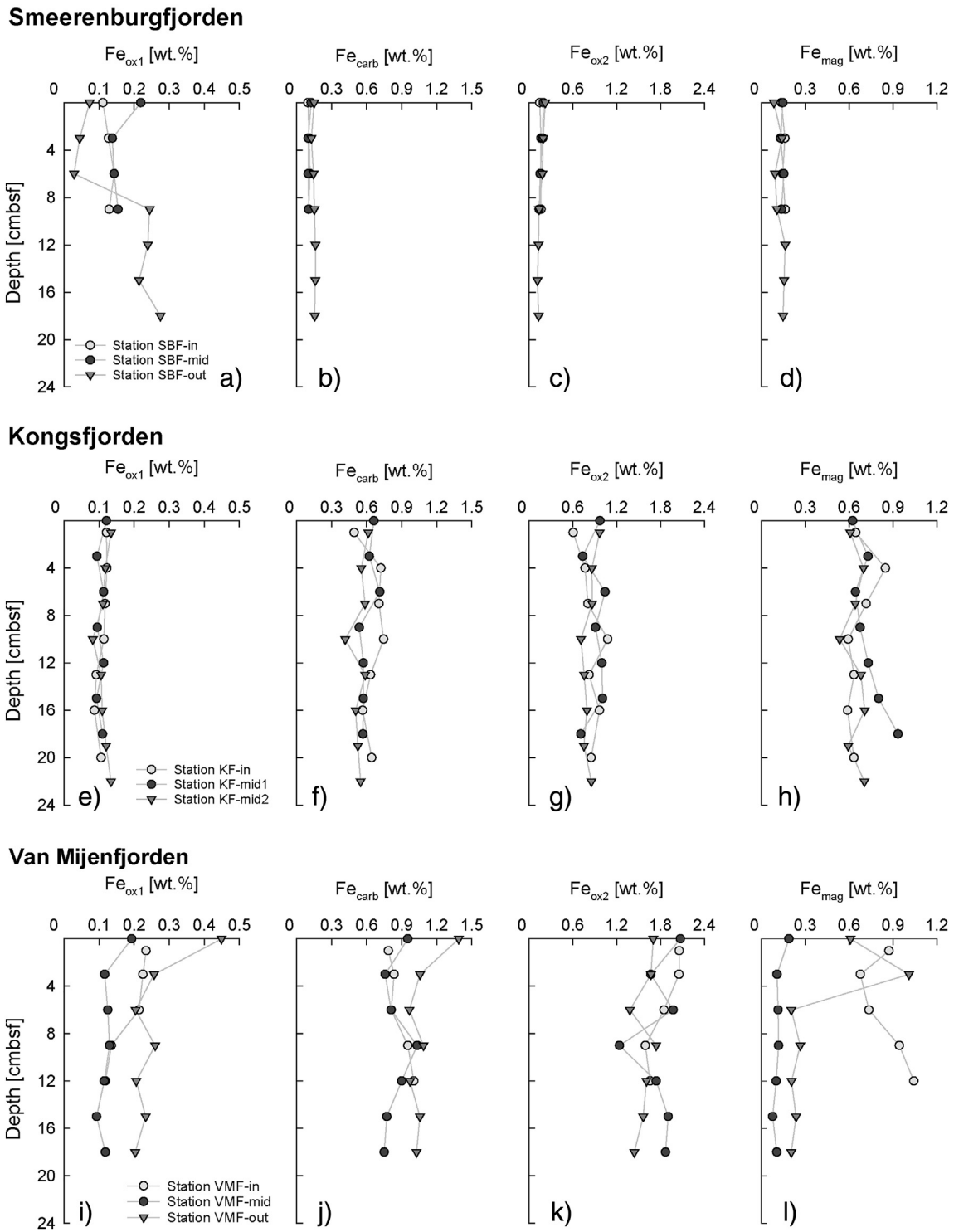

Fig. 2. Concentrations of amorphous and nanoparticulate iron (oxyhydr)oxide phases (Fe_{ox1}), iron bound in carbonates (Fe_{carb}), crystalline iron (oxyhydr)oxides (Fe_{ox2}), and magnetite (Fe_{mag}) with depth at the (a-d) Smeerenburgfjorden stations, (e-h) Kongsfjorden stations, and (i-l) Van Mijenfjorden stations.

impacted the sulfate concentration measurements. The isotope composition of sulfate (see below) does not scatter in a similar way, suggesting that the high sulfate concentrations did not jeopardize the isotope composition measurements. The origin for the artifact is not known; a potential cause could be errors during pipetting of the sample or addition of $ZnCl_2$ solution (dilution error). This error only affected the sulfate samples since the pore-water metal concentrations were analyzed in a different aliquot preserved with nitric acid.

At Smeerenburgfjorden station SBF-in, dissolved iron (Fe_{diss}) concentrations show a peak with a maximum value of 460 μM at ~6 cmbsf and decreasing concentrations below this depth (Fig. 6a). At SBF-mid, Fe_{diss} concentrations were < 50 μM. Concentrations at SBF-out were highest in the uppermost layer with a value of 130 μM and decreased to values < 20 μM below (Fig. 6a). At SBF-in, Mn_{diss} concentrations increased below 3 cmbsf to a maximum value of 50 μM before decreasing below this depth (Fig. 6b). At SBF-mid and SBF-out, Mn_{diss} concentrations were mostly < 10 μM.

At Kongsfjorden stations KF-in and KF-mid2, Fe_{diss} concentrations

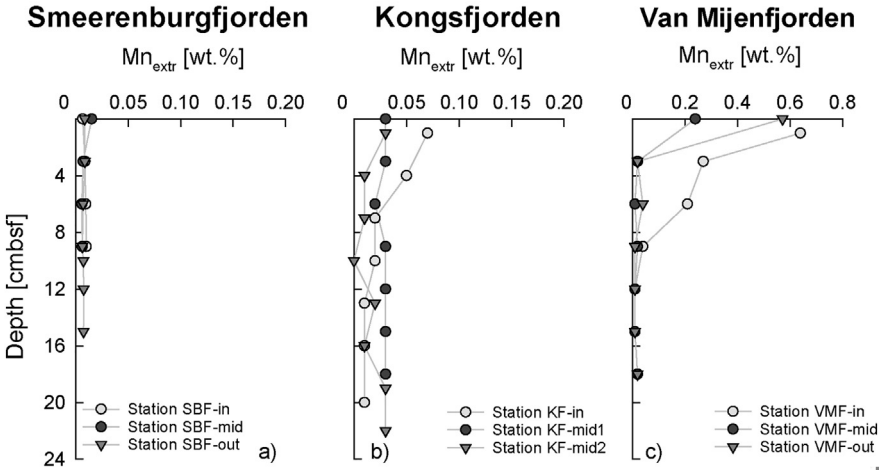

Fig. 3. Concentrations of extractable manganese phases (Mn_{extr}) with depth at the a) Smeerenburgfjorden stations, b) Kongsfjorden stations, and c) Van Mijenfjorden stations.

were between 20 and 240 μM but mostly remained at concentrations > 100 μM throughout the cores. Fe_{diss} concentrations at KF-mid1 were higher than at stations KF-in and KF-mid2, showing a steep increase in the top 3 cm and almost constant concentrations ~290 μM below (Fig. 6c). Mn_{diss} concentrations in Kongsfjorden sediments were highest at KF-in with maximum values ~36 μM at 7–10 cm, between 15 and 20 μM at KF-mid1, and lowest at KF-mid2 not exceeding 12 μM (Fig. 6d).

Van Mijenfjorden sediments display highest Fe_{diss} concentrations. At VMF-mid and VMF-out the Fe_{diss} concentrations were below detection in the surface sediment but increased steeply below 0.5 and 6 cmbsf, respectively, to concentrations exceeding 850 μM at VMF-mid and 460 μM at VMF-in (Fig. 6e). Fe_{diss} concentrations at VMF-out were in the range of 100–310 μM (Fig. 6e). Mn_{diss} concentrations at VMF-in and VMF-mid were an order of magnitude higher than concentrations at stations of the other fjords. At VMF-in, Mn_{diss} concentrations increased steeply in the surface 10 cm to values exceeding 650 μM, and decreased slightly below this depth (Fig. 6f). A similar but less pronounced trend was observed at VMF-mid where maximum concentrations reached 270 μM. At VMF-out Mn_{diss} concentrations were in the range of 60–100 μM (Fig. 6f).

4.3. Stable isotope composition

Sulfur and oxygen isotope values of pore-water sulfate display clear trends toward heavier isotopes with increasing burial depth at the Smeerenburgfjorden stations, with values reaching + 22.2‰ for $\delta^{34}S\text{-}SO_4^{2-}$ and + 11.0‰ for $\delta^{18}O\text{-}SO_4^{2-}$ in the deepest sediment section of SBF-in and similar distributions at the other Smeerenburgfjorden stations (Fig. 7a, b).

These trends are reflected in a concomitant linear relationship in the $\delta^{18}O\text{-}\delta^{34}S$ plot (Fig. 7c). Such trends are typical for sulfate removal by microbial sulfate reduction, and are expected to coincide with lower sulfate concentrations with increasing sediment depth (Böttcher et al., 1998; Böttcher et al., 1999; Aharon and Fu, 2000; Mandernack et al., 2003; Brunner et al., 2005; Antler et al., 2013). Due to the scatter in the sulfate concentration data, it is not possible to assess the degree of sulfate depletion at the time of sampling. However, from other campaigns, it is known that sulfate levels decrease from 27.8 mM at 1 cmbsf to 26.4 mM at 11cmbf at SBF-in and from 27.8 mM at 1 cmbsf to 23.8 mM at 30 cmbsf at SMF-out (Fig. S1a; Wehrmann et al., 2014); a similar distribution can be expected for the near-by SMF-mid.

At Kongsfjorden station KF-in sulfur and oxygen isotope values of sulfate changed little with depth, while at KF-mid1 and KF-mid2 enrichments in ^{34}S and ^{18}O were observed below 8 cmbsf and 13 cmbsf, respectively, with values of 22.6‰ for $\delta^{34}S\text{-}SO_4^{2-}$ and 11.0‰ for $\delta^{18}O\text{-}SO_4^{2-}$ in the deepest cored sediment at KF-2 (Fig. 7d, e). At Van Mijenfjorden stations VMF-in and VMF-mid sulfur and oxygen isotope values of sulfate also displayed little change with depth (Fig. 7g, h); subtle ^{34}S and ^{18}O enrichments were detected at VMF-out below 10 cmbsf (Fig. 7c, d).

We note that not all $\delta^{18}O$ and $\delta^{34}S$ values of sulfate closest to the sediment-water interface reflect modern seawater sulfate values (approximately 21‰ and 8.6‰). Such deviations in the oxygen and sulfur isotope composition of sulfate from seawater values can be caused by input of sulfate by glacial runoff, for example derived from the oxidation of pyrite within the bedrock. This process has been shown to produce sulfate that is isotopically enriched in ^{18}O and depleted in ^{34}S compared to seawater sulfate (Wadham et al., 2004).

The sulfur stable isotope profiles of sedimentary AVS and CRS at SBF-out were almost identical, with values mostly between − 20 and − 30‰, while $\delta^{34}S\text{-}S_{org}$ determined at 10 cmbsf was ~ − 8‰ (Fig. 8a). An offset between the sulfur isotope composition of AVS and CRS of ~ + 10‰ was observed below 8 cm at KF-in and VMF-out (Fig. 8b, c). Sulfur isotope values of S_{org} were ~0‰ at KF-mid2 and ~ − 4‰ at VMF-out and remained almost constant with depth (Fig. 8b, c).

At VMF-out, the lowest $\Delta^{33}S$ values were detected for sulfate (0.012–0.030‰), followed by the $\Delta^{33}S$ values for CRS (0.028–0.076‰); the AVS pool had the highest $\Delta^{33}S$ values, in the 0.076–0.118‰ range (Table 4).

5. Discussion

5.1. Input of glacially derived iron oxide phases, organic matter, and CRS to fjord sediments

Glacially influenced fjords often receive a high loading of dissolved and particulate iron from glacial runoff (e.g., Statham et al., 2008; Raiswell et al., 2006, 2008; Bhatia et al., 2013; Wadham et al., 2013; Hawkings et al., 2014). The extent of this input is strongly controlled by discharge volume and suspended load of the glacial runoff, composition of the subglacial bedrock, and diagenetic processes in glacial floodplains (Wehrmann et al., 2014; Hodson et al., 2016). The three investigated fjords display a distinct trend in the sedimentary concentrations of easily reducible and reducible particulate iron phases from lowest contents at Smeerenburgfjorden to greatest contents at Van Mijenfjorden. These phases typically encompass amorphous and nanoparticulate iron (oxyhydr)oxide phases (Fe_{ox1}), e.g., ferrihydrite (Raiswell et al., 2010) and crystalline iron (oxyhydr)oxides (Fe_{ox2}) such as goethite (Mehra and Jackson, 1960; Lord, 1980; Poulton and Canfield, 2005; Fig. 2). This trend likely reflects differences in the iron content of the local bedrock, which ranges from (low-iron) gneisses and migmatites at Smeerenburgfjorden to sandstones and shales at Kongsfjorden and Van Mijenfjorden (see Table 1 for details on bedrock

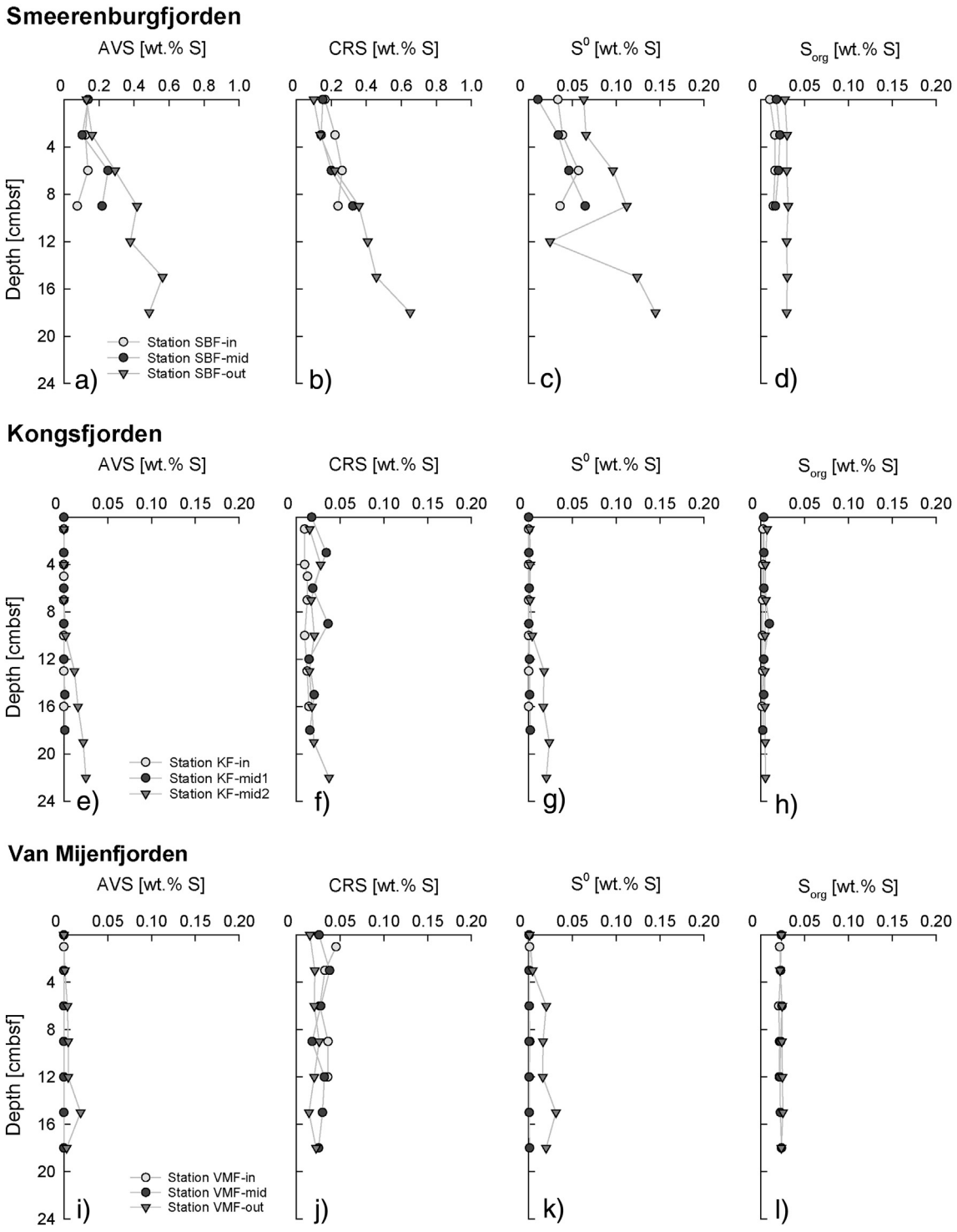

Fig. 4. Concentrations of acid volatile sulfide (AVS), chromium reducible sulfur (CRS), elemental sulfur (S^0), and organic matter-bound sulfur (S_{org}) with depth at the (a-d) Smeerenburgfjorden stations, (e-h) Kongsfjorden stations, and (i-l) Van Mijenfjorden stations. Note difference in scale for Smeerenburgfjorden AVS and CRS plots as compared to Kongsfjorden and Van Mijenfjorden. All values are in wt% dry weight.

compositions), and variations in the size of the glacial catchment areas (Table 1; Wehrmann et al., 2014).

The varying imprint of the local glaciers on the sediment characteristics of the three fjords is also observed in different TOC contents and C/N ratios (Table 3; Fig. 3). The more limited runoff of meltwater from glaciers into Smeerenburgfjorden and the faster exchange of seawater with the open ocean results in sedimentary C/N ratios that are typical for organic matter derived from marine phytoplankton (Meyers, 1994). In contrast, higher sedimentary C/N ratios at Kongsfjorden and Van Mijenfjorden are likely indicative of the additional input of terrestrial organic matter (OM; Hebbeln and Berner, 1993; Wagner and Dupont, 1999; Meyers, 1994; Wehrmann et al., 2014; Koziorowska et al., 2016). This terrestrial organic matter can be fresh terrestrial biomass, soil-derived, coal-derived or ancient OM, which is likely derived from pre-aged soil or potentially ancient marine sediments presently covered by glaciers (Kim et al., 2011; Kuliński et al., 2014; Koziorowska et al., 2016; Zaborska et al. in press). A previous study suggested that the contribution of (modern) soil-derived OM to Kongsfjorden sediments is of minor

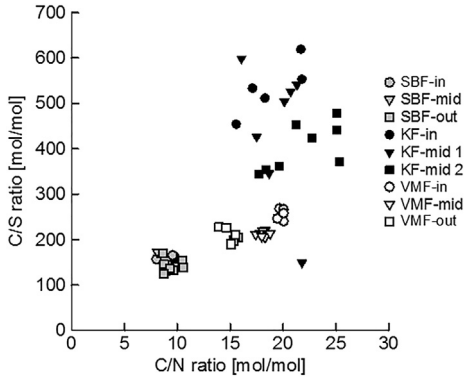

Fig. 5. Plot of average molar organic carbon to nitrogen ratios (C/N) versus molar organic carbon to organic sulfur ratios (C/S) for each station in the three investigated fjords.

importance, but that ancient OM contributes up to 91% of sedimentary OM in the innermost Kongsfjorden area at the Kongsvegen glacier front, and 40–60% to sedimentary OM in the inner Kongsfjorden area where KF-mid1 and KF-mid2 are located (Kim et al., 2011). Concomitantly, marine OM constitutes < 20% of the sedimentary OM in the inner Kongsfjorden area (Kim et al., 2011). Although values for the contribution of terrestrial OM to sediments in Van Mijenfjorden are not available, a recent study on Adventfjorden, which is located to the north of Van Mijenfjorden and characterized by the same bedrock composition of the Adventdalen and Van Mijenfjorden Groups (Dallmann, 1999), provides evidence for a terrestrial OM contribution to the sedimentary OM pool of 82–83% (Koziorowska et al., 2016). Seaward increases in TOC contents at Smeerenburgfjorden and Kongsfjorden likely reflect increasing primary productivity in the water column away from turbid meltwater (Hop et al., 2002) and decreasing dilution of the total organic carbon pool by glacially derived material, and thus likely also a decreasing contribution of terrestrial TOC to the total TOC pool, especially at Kongsfjorden (Zaborska et al. in press). Similarly, the contribution of terrestrial TOC to Van Mijenfjorden also decreases seaward as indicated by the decreasing C/N ratio, although TOC values slightly decrease along the fjord axis (Table 3). The terrestrial, ancient organic matter is likely very recalcitrant, while the marine organic matter is more easily degradable. The differences in the composition of organic matter for the different fjords become most evident in C/S vs. C/N plots (Fig. 5). For Smeerenburgfjorden all data fall in a small cluster with low C/N and C/S ratios (7–12, and 125–175, respectively). For Van Mijenfjorden, the data fall in distinct clusters with VMF-out (14–16, and 190–230, respectively) plotting closest to the Smeerenburgfjorden cluster, followed by VMF-mid, and VMF-in (19–20, and 240–270, respectively). The data scatter most strongly for Kongsfjorden, with C/N ratios of 16–25 and C/S ratios of 340–620 (with one exception of 120) for bulk sediment.

In light of these findings, it is not surprising that a portion of the organically bound sulfur (S_{org}) and CRS (i.e., pyrite) is likely also of detrital origin (see Brüchert et al., 2001; Wehrmann et al., 2014). Pyrite and organically bound sulfur are present in all surface sediments, and for the majority of the investigated stations there is neither evidence for an increase in CRS contents with depth (KF-in, KF-mid1, and all sites in Van Mijenfjorden; Fig. 4), nor is there evidence for an increase in organic matter-bound sulfur with depth at any of the stations (Fig. 4). Wehrmann et al. (2014) identified highly variable sulfur isotope values of CRS in surface sediments of different stations within Kongsfjorden as evidence for the input of detrital pyrite from varying bedrock sources (medium-grade metamorphic rocks of Middle Proterozoic Age vs. Devonian sandstones vs. Late Paleozoic sedimentary rocks). We collected a small set of samples of surrounding detrital source rocks in Zeppelinfjället, located on the southern side of Kongsfjorden, and determined their sulfur isotope composition. Results show that weathering and runoff of pyrite from these rocks delivers an isotopically heavy fraction of pyrite to the fjord sediment that can help explain the comparably

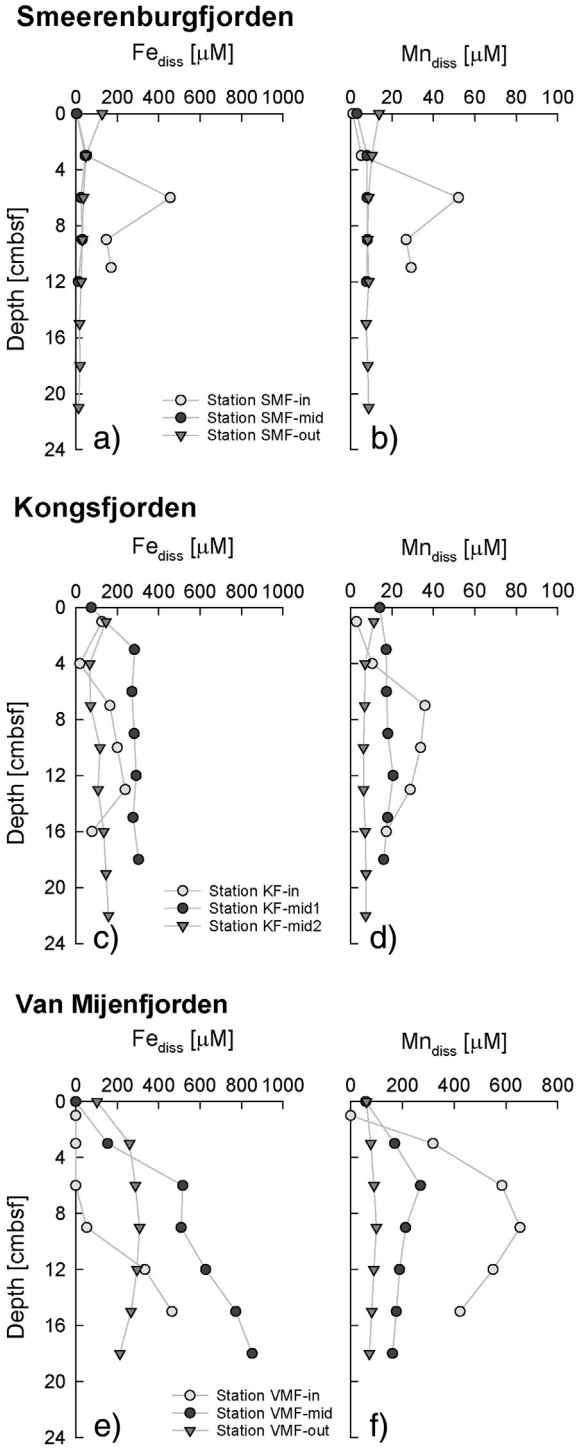

Fig. 6. Pore-water dissolved iron (Fe_{diss}) and manganese (Mn_{diss}) concentrations with depth at the (a, b) Smeerenburgfjorden stations, (c, d) Kongsfjorden stations, and (e, f) Van Mijenfjorden stations.

heavy sedimentary sulfur isotope values of pyrite compared to the AVS pool at KF-mid2, and – due to the same mechanism – at VMF-out (Table 5; Fig. 8). This does not mean that no new CRS or organically bound sulfur is generated within the sediment at the aforementioned stations, but it demonstrates that a fraction of the sulfur is detrital and may mask signals derived from authigenic CRS and S_{org} (Fig. 4). This complication is important, because compared to other sulfur compounds, such as iron monosulfide or elemental sulfur, organically bound sulfur and CRS have a greater potential to be preserved over long timescales, and become part of the geological archive.

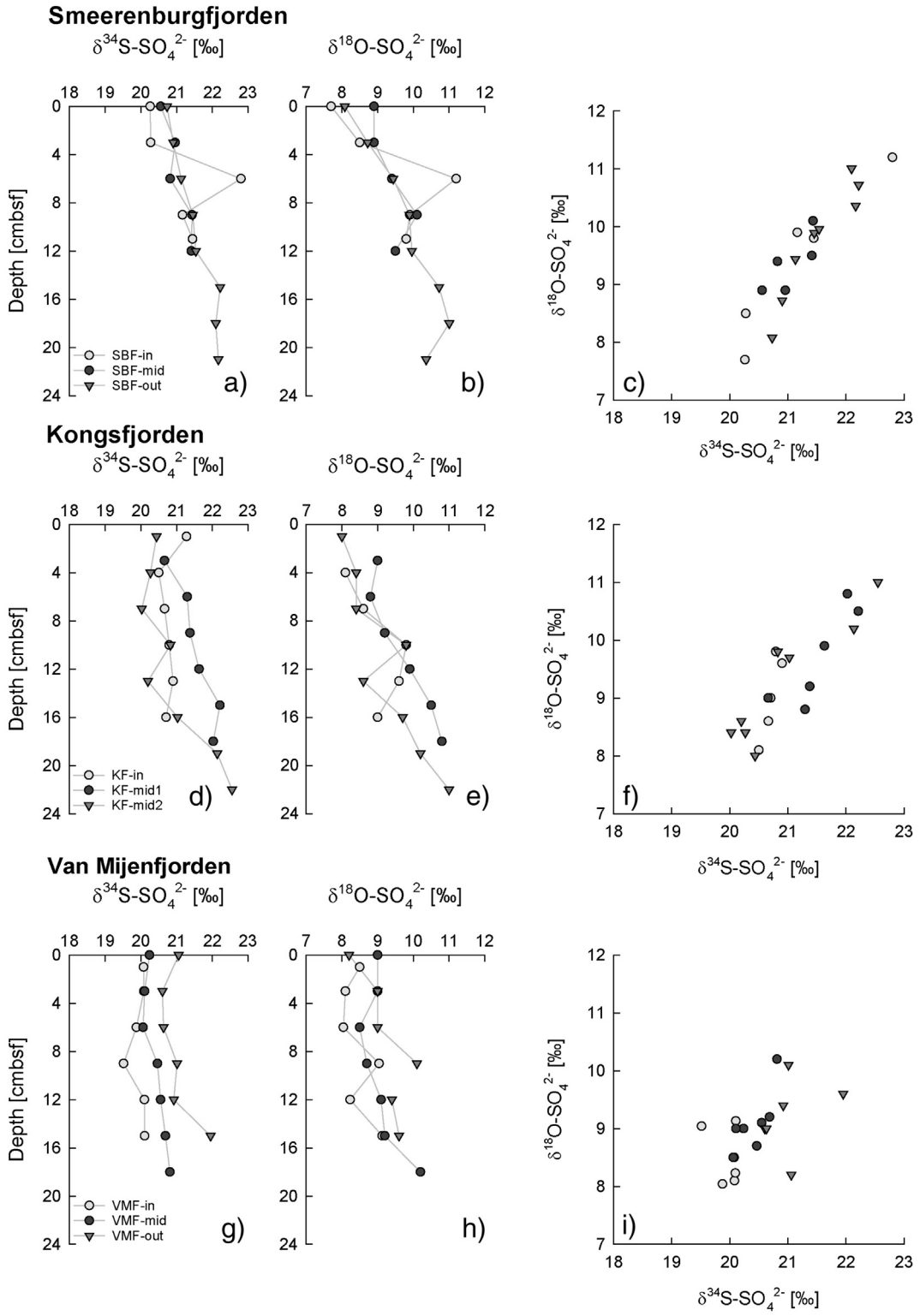

Fig. 7. Stable sulfur and oxygen isotope composition of pore-water sulfate with depth and $\delta^{18}O\text{-}SO_4$ versus $\delta^{34}S\text{-}SO_4$ plots at (a-c) Smeerenburgfjorden stations, (d-f) Kongsfjorden stations, and (g-i) Van Mijenfjorden stations.

5.2. Role of iron and manganese oxides in controlling biogeochemical reactions of the sedimentary sulfur cycle

Amongst the key questions regarding the biogeochemical sulfur and iron cycling in the investigated fjords are (i) how do variations in the extent and reaction pathways of sulfur cycling linked to iron and other potential oxidants in the surface sediment modulate the content and isotope signature of sulfur compounds, and (ii) how are associated biogeochemical signatures preserved on different timescales? A straightforward way to find a preliminary answer to the first question is to interpret patterns in $\delta^{18}O$ vs. $\delta^{34}S$ plots of pore-water sulfate (Fig. 7c, f, i). Such graphs provide several pieces of information; i) for most sites, the spread in the data exceeds the measurement error (one exception is VMF-in) and ii) enrichments in ^{18}O tend to coincide with enrichments

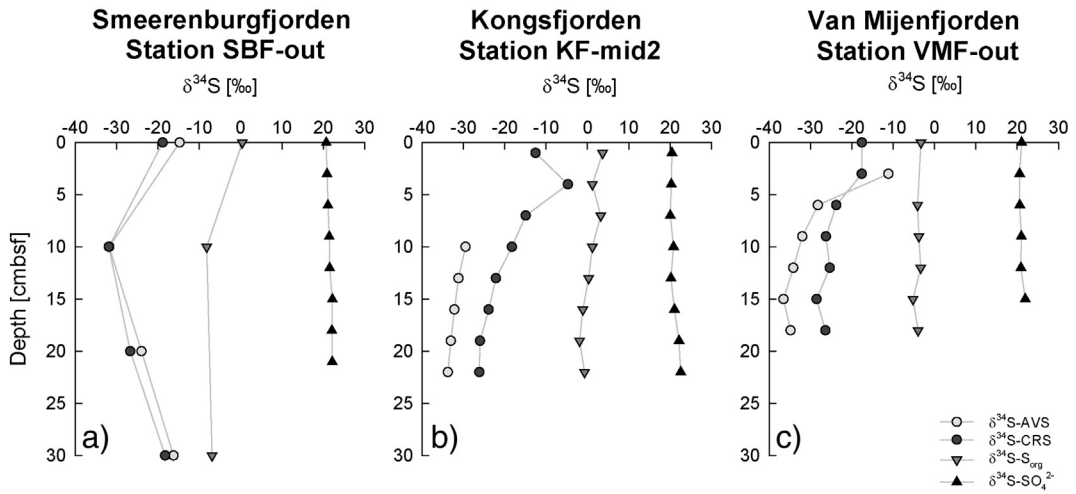

Fig. 8. Sulfur isotope composition of AVS, CRS, S_{org}, and sulfate at a) Smeerenburgfjorden Station SMF-out, b) Kongsfjorden Station KF-mid2, and c) Van Mijenfjorden Station VMF-out.

Table 4
$\Delta^{33}S$ values for sulfate, acid-volatile sulfide (AVS), and chromium reducible sulfur (CRS) at Station VMF-out with depth.

Sediment depth	$\Delta^{33}S\text{-}SO_4^{2-}$	$\Delta^{33}S$-AVS	$\Delta^{33}S$-CRS
0			0.001
3	0.016		0.028
6	0.015		0.072
9	0.023	0.107	0.076
10	0.012		
12	0.030	0.076	0.035
15	0.027	0.118	0.059
18		0.111	0.062

Table 5
Sulfur isotope composition of chromium reducible sulfur ($\delta^{34}S$-CRS) of rock samples collected in Zeppelinfjället, Kongsfjorden.

Sample description	$\delta^{34}S$-CRS
Gneiss	17.0
Marlstone	6.5
Basaltic Lava	− 0.1
Fine-grained red siltsone, weakly metamorphosed	− 5.0
Coal	2.2
Basaltic Lava with idiomorphic inclusions	0.4
Pyroclastic breccia	38.4
Pegmatite with inclusions (pyrite, chlorite, epidote or sulfur)	15.1
Fine-grained grey-green siltsone, weakly metamorphosed	− 1.2

in ^{34}S. The latter is a trend typical for sulfate reduction in marine sediments (Böttcher et al., 1998; Böttcher et al., 1999; Aharon and Fu, 2000; Mandernack et al., 2003; Brunner et al., 2005; Antler et al., 2013). The former simply implies that some form of sulfur cycling, including possibilities such as reductive, oxidative, diffusive or advective turnover, must be active to result in a data spread that is larger than the measurement error. From this quick assessment one can conclude that sulfur cycling must be taking place at most of the investigated sites, however, it does not provide insight into the mechanics or rates of this cycling. Here, the gathered holistic data set with the observed differences in sedimentary iron (and manganese) oxide concentrations amongst the three fjords allows us to investigate potential variations in the biogeochemical interactions of the S-Fe-Mn system as a function of glacially derived iron and manganese oxide availability in fjord sediments, and to decipher the resulting imprint on sulfur (and oxygen) isotopic signals of a range of sulfur species. Based on the relationship between iron and sulfur species observed at the different sites, we group these nine stations into the three categories described below.

5.2.1. Low pore-water iron, high sedimentary sulfur (low-Fe^{2+}/high-S) end-member stations in Smeerenburgfjorden

At Smeerenburgfjorden stations SBF-mid and SBF-out, pore-water iron and manganese concentrations show a sharp decline below the top 3 cm to values < 40 μM (Fig. 6a, b); sedimentary AVS, CRS, and S^0 concentrations increase below this depth (Fig. 4a–c). At station SBF-in, pore-water metal concentrations remain slightly elevated (Fig. 6a, b), CRS and S^0 concentrations also increase with depth (Fig. 4a–c).

At the three Smeerenburgfjorden stations, Fe^{2+} is likely produced during dissimilatory iron reduction in the topmost layer of the sediment and subsequently scavenged by reactions with sulfur species in deeper sediment. Previous studies at SBF-out have shown that dissimilatory iron reduction contributes 13% to organic carbon mineralization in the top 10 cm of the sediment and that elevated sulfate reduction rates of ~15 nmol cm^{-3} d^{-1} are found below 2 cmbsf (Vandieken et al., 2006a). Sulfide, produced during organoclastic sulfate reduction within and below this surface zone, reacts with Fe^{2+} to form iron monosulfide (AVS) (Eq. (3)):

$$H_2S + Fe^{2+} \rightarrow FeS + 2\,H^+ \quad (3)$$

When Fe^{2+} is depleted, sulfide can reduce reactive iron mineral phases with subsequent AVS and S^0 formation in a two-step process involving the production of Fe^{2+} as an intermediate, following the net equation (Eq. (4); Canfield, 1989):

$$3\,H_2S + 2\,FeOOH \rightarrow 2\,FeS + S^0 + 4\,H_2O \quad (4)$$

Increasing sulfide concentrations from 2 μM at 13 cmbsf to 306 μM at 43 cmbsf have previously been reported for sediments at SBF-out while no sulfide was detected at SBF-in (Wehrmann et al., 2014). Zero-valent sulfur, and ultimately S^0 is likely also formed by incomplete oxidation of sulfide with nitrate (Schippers and Jørgensen, 2001). The formation of S^0 is evidenced by increasing S^0 concentrations with depth at all Smeerenburgfjorden stations (Fig. 4c). Both AVS and S^0 can subsequently take part in pyrite formation. Iron monosulfide, (i.e. AVS) can react directly with sulfide to form pyrite (i.e. CRS) following Eq. (5) (Rickard and Luther, 1997),

$$FeS + H_2S \rightarrow FeS_2 + H_2 \quad (5)$$

or S^0 can interact with sulfide to form polysulfides, which then take part in a reaction with AVS to form pyrite (Luther, 1991; Schoonen and Barnes, 1991; Wilkin and Barnes, 1996).

Additionally, polysulfides and other intermediate sulfide oxidation products can catalyze the sulfurization of labile organic matter to OSC (e.g., Vairavamurthy and Mopper, 1987; Sinninghe Damste and de

Leeuw, 1990; Werne et al., 2000, 2008). Recent studies have shown that this process appears to be prevalent in sediment zones where the presence of S^0 and hydrogen sulfide promote the formation of polysulfides (e.g., Werne et al., 2008; Riedinger et al., 2017). These settings are similar to the deeper sediments at the Smeerenburgfjorden stations, especially SBF-out. While an increase in S_{org} concentrations is not observed at this station (Fig. 4), $\delta^{34}S$- S_{org} values indicate that organically bound sulfur becomes slightly more depleted in ^{34}S with depth (Fig. 8a). To explain similar trends in surface sediments of a Scottish fjord, Bottrell et al. (2009) proposed that some sedimentary organosulfur compounds may undergo exchange with dissolved H_2S, or that there is a steady state between the mineralization of original OSCs and the formation of new compounds that are characterized by a lighter sulfur isotope composition.

Differences in pore-water iron and sulfide concentrations between the three stations can be explained by higher contents of reactive iron phases at SBF-in compared to SBF-mid and SBF-out, as Wehrmann et al. (2014) previously showed that iron oxide accumulation rates in western Svalbard fjords generally decrease with increasing distance from the glaciers. This difference in iron oxide accumulation likely extends the zone of dissimilatory iron reduction in the surface zone of SBF-in while at the same time providing a larger amount of reducible iron oxide phases for reaction with sulfide. Due to the very low concentration of Mn_{extr}, biogeochemical manganese cycling is likely of limited importance in Smeerenburgfjorden sediments (Fig. 3a). This is in accordance with the results from incubation experiments with sediment from SBF-out by Vandieken et al. (2006a) who found low, yet detectable Mn(IV) reduction, but only in the uppermost 1.5 cm of the sediment.

At the three Smeerenburgfjorden stations the sulfur transformations leave a distinct imprint in the isotope composition of sulfate, with enrichments in ^{34}S and ^{18}O with depth (Fig. 7a, b). This pattern is typical for marine sediments with ongoing sulfate reduction in the upper sulfate zone (Aharon and Fu, 2000; Mandernack et al., 2003; Brunner et al., 2005; Antler et al., 2013). At SBF-out, the sulfur isotope composition of organically bound sulfur, AVS and CRS show a curious pattern (Fig. 8a). In the top 10 cm these sulfur phases become more depleted in ^{34}S with depth. In the following interval down to 30 cm this trend is reversed for AVS and CRS. These trends are best explained by two contributing factors. First, as substantial amounts of CRS and AVS are formed with depth, i.e., below the surface few cm, the relative contributions of these authigenic phases to the total CRS and AVS pools increase compared to their detrital counterparts and the overall sulfur isotope signals show stronger overprint by the authigenic phases. Second, the trends in the sulfur isotope signatures of AVS and CRS with depth reflect the formation of ^{34}S–depleted sulfide that becomes less depleted in the heavy isotope with depth. Using the sulfur isotope composition of AVS as proxy for the isotope composition of sulfide (sulfur isotope effects related to the precipitation of iron monosulfides and pyrite are assumed to be small, i.e. < 1‰; Wilkin and Barnes, 1996; Böttcher et al., 1998; Butler et al., 2004), one expects that sulfide formed at SMF-out has a sulfur isotope composition of approximately − 30‰ at 10 cm depth and − 20‰ at 30 cm depth. With a $\delta^{34}S$ of approximately + 21‰ for sulfate, this would correspond to a change in sulfur isotope fractionation ($\varepsilon^{34}S$) from 50‰ to 40‰. The net sulfur isotope fractionation by sulfate reduction in marine surface sediments is typically up to ~45‰ (e.g. Kaplan and Rittenberg, 1964; Rees, 1973, Brunner and Bernasconi, 2005; Farquhar et al., 2008). It can exceed 70‰ (Brunner and Bernasconi, 2005; Canfield et al., 2010a, 2010b; Sim et al., 2011); however, such large sulfur isotope discrimination may be typical for deeper and more energy-limited sediments (Wortmann et al., 2001; Rudnicki et al., 2001; Wehrmann et al., 2015). Energy limitation due to the refractory nature of organic matter is expected to increase with sediment depth, thus a trend from larger to smaller sulfur isotope fractionation is rather unexpected. A more likely explanation is that the sulfur isotope fractionation for organoclastic sulfate reduction at SBF-out is < 40‰, and that this fractionation is overprinted by sulfur isotope fractionation related to the disproportionation of S^0, especially below the surface few cm where the activity of bioturbating and bioirrigating organisms provides ample oxidants for the oxidation of intermediate sulfur species to sulfate (Habicht and Canfield 2001). Sulfur disproportionation drives the sulfur isotope composition of sulfide to more ^{34}S–depleted values (Jørgensen, 1990; Canfield and Thamdrup, 1994; Böttcher et al., 2001; Habicht and Canfield, 2001; Böttcher et al., 2005). At SBF-out, the maximum sulfur isotope offset between sulfate and AVS at 10 cm depth and the increase of S^0 concentrations with depth may suggest that disproportionation rates are highest immediately below the maximum bioturbation depth and decrease below. This decrease may be the result of the inhibition of sulfur disproportionation due to the presence of sulfide in the pore-water (Lovley and Phillips, 1994; Finster et al., 1998).

5.2.2. High pore-water iron, low sedimentary sulfur (high Fe^{2+}/low-S) end-member stations VMF-in and VMF-mid in Van Mijenfjorden and KF-in and KF-mid1 in Kongsfjorden

At VMF-mid, KF-in and KF-mid1, pore-water iron and, to a lesser extent, manganese concentrations remain high throughout the investigated sediment interval (Fig. 6c–f). VMF-in displays an increase in pore-water manganese concentrations below 2 cmbsf followed by a steep increase of pore-water iron concentrations below 8 cmbsf (Fig. 6e, f). At all four stations sedimentary AVS, CRS and S^0 concentrations remain low throughout the investigated sediment depth (Fig. 4e–g). Sulfate concentrations at KF-in (Wehrmann et al., 2014), KF-mid1, and VMF-in (2016 cores, Fig. S1) show < 1 mM variation in the top 30 cm of the sediment. These observations indicate that at these stations either little sulfate is turned over and/or that any produced sulfide, including FeS, is re-oxidized by nitrate, highly reactive iron, or manganese oxides to intermediate sulfur species and sulfate. In the first case, organic carbon mineralization primarily proceeds via dissimilatory iron and manganese oxide reduction while sulfate reduction only takes place deeper in the sediment. This hypothesis is supported by sulfate reduction rates at station KF-mid1 (Jørgensen, unpublished data) analyzed using the ^{35}S–radiotracer technique during a previous expedition which were extremely low at all depths (< 3 nmol cm^{-3} d^{-1}). In the latter case, the absence of the metastable sulfur intermediate S^0 would indicate that high availability of oxidants drives complete re-oxidation of reactive sulfur to sulfate. This interpretation is also supported by the observation that the CRS concentrations do not increase with depth. Since nitrate is likely limited to the surface 1–3 cm of the sediment in these fjords (Kostka et al., 1999; Canion et al., 2014), we suggest that such potential rapid oxidation of reduced sulfur – if present – is primarily a result of the high availability of easily reducible and reducible iron oxide below the topmost 3 cm of the sediment (Fig. 2e, g, i, k; Canfield and Thamdrup, 1996). The activity of bioirrigating organisms may promote the downward transport of oxygen, which then takes part in the recycling of oxidant such as iron below the depth of diffusive oxygen penetration (< 1 cm; Kostka et al., 1999; Berner and Westrich, 1985). The formation of organically bound sulfur at these stations is likely low, as evidenced in constant S_{org} concentration profiles primarily reflecting detrital organic matter-bound sulfur input (Fig. 4). This can be attributed to the absence of sulfide from the pore-water which likely limits the formation of polysulfide and subsequent organic matter sulfurization (Werne et al., 2003, 2008; Riedinger et al., 2017; Hartgers et al., 1997).

Additionally, at VMF-in and VMF-mid, the sulfur and oxygen isotopic composition of pore-water sulfate changes very little with depth (Fig. 7g, h). This pattern can again be explained by (i) low sulfate reduction rates in the top 24 cm of the sediment investigated at these stations and/or (ii) the complete oxidation of produced sulfide and potentially intermediate sulfur species to sulfate by abiotic and biotic oxidation pathways, e.g., involving nitrate and reactive iron (oxyhydr) oxide –potentially partially sustained by oxygen delivery via

bioirrigation– without any burial as AVS or pyrite. At extremely low rates of sulfate reduction (hence a large pool of pore-water sulfate) in surface sediments, changes in the sulfur and oxygen isotopic composition of sulfate are likely undetectable, i.e., within the error of the measurement. The oxidation of sulfide and potentially intermediate sulfur species, produced during dissimilatory sulfate reduction, back to sulfate by abiotic and biotic oxidation pathways also helps to attenuate any potential sulfur isotope effects generated by sulfate reduction. It results in the re-introduction of produced light sulfide back into the sulfate pool with only small fractionation effects (i.e., closed-system conditions; Fry et al., 1984, 1988; Kelly, 2008; Toran and Harris, 1989; Hubert et al., 2009; Poser et al., 2014). The processes that affect the oxygen isotope composition of sulfate are somewhat more intricate. Dissimilatory sulfate reduction drives the oxygen isotope of sulfate toward the equilibrium oxygen isotope offset between sulfate and water (Mizutani and Rafter, 1973; Fritz et al., 1989; Brunner and Bernasconi, 2005, Brunner et al., 2005). Abiotic and biotic sulfide oxidation pathways are generally associated with small oxygen isotope fractionation effects and thus tend to contribute sulfate to a sulfate oxygen isotope pool that has an isotope composition close to the one of ambient water (Toran and Harris, 1989; Balci et al., 2007; Brunner et al., 2008; Thurston et al., 2010; Poser et al., 2014). In combination, these effects may cause the absence of a clear oxygen isotope trend at stations VMF-in and VMF-mid (Fig. 7g–i).

At KF-in and KF-mid1, the range of isotope values is somewhat larger, and shows a subtle increase in $\delta^{18}O$ and $\delta^{34}S$ with depth (Fig. 7d–f). At KF-1 the oxygen isotope enrichment is approximately four times larger than the sulfur isotope enrichment. The described combination of low rates of sulfate reduction (which drive a more rapid $\delta^{18}O$ than $\delta^{34}S$ increase; Antler et al., 2013) and extensive oxidation of produced sulfide and potentially intermediate sulfur species to sulfate is likely also responsible for the isotope pattern observed at these sites. However, sulfur disproportionation may also occur at these stations, in particular at KF-in. When sulfur oxidation operates predominantly via sulfur disproportionation, and the oxygen isotope composition of sulfate is driven toward the equilibrium isotope value by both sulfur disproportionation and sulfate reduction, a strong change in $\delta^{18}O$ with a concomitant small change in $\delta^{34}S$ can be observed.

The opposing iron and manganese profiles at VMF-in suggest that Fe^{2+} diffusing upward at this site is oxidized by reaction with manganese oxides following Eq. (6) (Aller, 1994).

$$MnO_2 + 2\,Fe^{2+} + H_2O \rightarrow Mn^{2+} + 2\,FeOOH + 2\,H^+ \quad (6)$$

Furthermore, at all Van Mijenfjorden stations, Mn_{extr} is highly enriched in the top 4 cm of the sediment which provides evidence for the re-oxidation of Mn^{2+}, produced during dissimilatory manganese oxide reduction and the reaction of Fe^{2+} with manganese oxides, by downward diffusing oxygen close to the sediment surface (Aller, 1990; Calvert and Pedersen, 1993; Canfield et al., 1993).

5.2.3. Elevated pore-water iron and sedimentary S^0 values - the intermediate stages at Kongsfjorden KF-mid2, and Van Mijenfjorden VMF-out

At Kongsfjorden KF-mid2, and Van Mijenfjorden VMF-out, elevated pore-water iron concentrations (Fig. 6c, e) and generally low AVS and CRS concentrations (Fig. 4e, f, i, j) indicate extensive sulfide and FeS re-oxidation by nitrate, highly reactive iron-, or manganese oxides to polysulfides, S^0 or sulfate (e.g., Aller and Rude, 1988; Schippers, 2004; Jørgensen and Kasten, 2006). Ferrous iron is mainly derived from dissimilatory iron reduction, as previous measurements in the vicinity of VMF-out showed that this mineralization pathway contributes 26% to organic carbon mineralization in the top 10 cm of the sediment (Kostka et al., 1999; Nickel et al., 2008). In contrast to the setting described for the *high-Fe^{2+}/low-S end-member stations*, S^0 accumulates in the sediment at these stations, though the depth of initial S^0 increase varies amongst the stations. We propose that in this intermediate setting the availability of oxidants to facilitate the further oxidation of S^0 to sulfate is lower, allowing for the accumulation of S^0.

Lower availability of easily reducible and reducible iron oxide phases at Kongsfjorden station KF-mid2 and Van Mijenfjorden station VMF-out is likely the result of lower iron oxide accumulation rates compared to the other stations in the fjords, due to their more distal locations from the glacial sources.

A trend to lower Fe_{ox1} concentrations with depth is observed at VMF-out but not at the Kongsfjorden stations (Fig. 2e, i). It is known, however, that the solubility (and thus reactivity) of ferrihydrite, an important component of the sedimentary Fe_{ox1} pool, decreases during aging due to, amongst other factors, changes of crystal size, morphology, reactive site density, and aggregation (Hyacinthe and Van Cappellen, 2004; Raiswell et al., 2010). Aging and thus a decrease in solubility of the Fe_{ox1} pool may offer an explanation for a decrease of Fe_{ox1} availability/reactivity toward intermediate sulfur species at the more outward fjord stations.

The sulfur and oxygen isotopic values of sulfate at KF-mid2 and VMF-out display a heterogeneous picture, encompassing the spread of patterns between the *low-Fe^{2+}/high-S end-member* with a distinct enrichment in ^{18}O and ^{34}S at depth for KF-mid2 and the *high Fe^{2+}/low-S end-member* with increasing $\delta^{18}O$ with depth and little variation in $\delta^{34}S$ (with one exception at the bottom of the sediment profile at 25 cm) for VMF-out (Fig. 7).

At station VMF-out the sulfur isotope offset between sulfate and AVS is ~31‰ at a sediment depth of 3 cmbsf, and increases rapidly with depth to up to ~57‰ in the deepest sediment layers, a trend that appears to occur also at KF-mid2 (Fig. 8b, c). It can be argued that below the bioturbated zone, the microbial community in the sediment becomes more energy-limited (i.e. organic matter is highly refractory) which could induce stronger sulfur isotope fractionation (e.g. Canfield, 2001; Wing and Halevy, 2014). In this scenario, the differences in the sulfur isotope offsets between SBF-out, KF-mid2, and VMF-out (Fig. 8) could be attributed to the different types of organic matter in the fjords, which is evidenced by differences in C/N and C/S ratios (Fig. 5). Alternatively, the change in the isotope offset can be interpreted as the result of the competition between sulfur oxidation (occurs in shallow sediments; no imprint on the isotope composition of AVS) and sulfur disproportionation (occurs in deeper sediments, where availability of oxidants becomes more limited). Sulfur oxidation does not strongly fractionate isotopes (e.g., Toran and Harris, 1989; Fry et al., 1984, 1985; Kelly et al., 1997; Zerkle et al., 2009; Brabec et al., 2012), and thus does not overprint the isotope signature of sulfate reduction, whereas the sulfur disproportionation causes an enhanced depletion in ^{34}S in the produced sulfide.

The difference between $\Delta^{33}S$ values of CRS and sulfate is smaller than typical $\Delta^{33}S$ values expected for fractionation driven by sulfate reduction, and one of the data points falls outside the range of isotopic compositions calculated by Farquhar et al. (2007) for the Brunner and Bernasconi (2005) model for microbial sulfate reduction alone (Fig. 9). However, in this setting the CRS values have to be treated with caution as a substantial part of the CRS is of detrital origin (see Section 5.3.1). Concomitantly, the sample that plots outside of the typical sulfate reduction-range is from the shallowest depth, where one would expect the highest ratio of detrital to authigenic pyrite. Consequently, to assess if in these fjord settings processes other than sulfate reduction play an important role in sulfur cycling, such as disproportionation (Johnston et al., 2005) or sulfur oxidation (Zerkle et al., 2009), it is more appropriate to use $\Delta^{33}S$ values of AVS. Intriguingly, the $\Delta^{33}S$ values of AVS fall within a typical range for microbial sulfate reduction, and provide little evidence for oxidative sulfur cycling (Table 4).

Overall, the high availability of reactive iron oxides in the Svalbard fjords represents a key driver for geochemical processes in the sediment by: 1) directly facilitating dissimilatory iron reduction, 2) promoting oxidative, “cryptic” pathways in the sedimentary sulfur cycle, and 3) preventing the sulfurization of organic matter despite an active sulfur

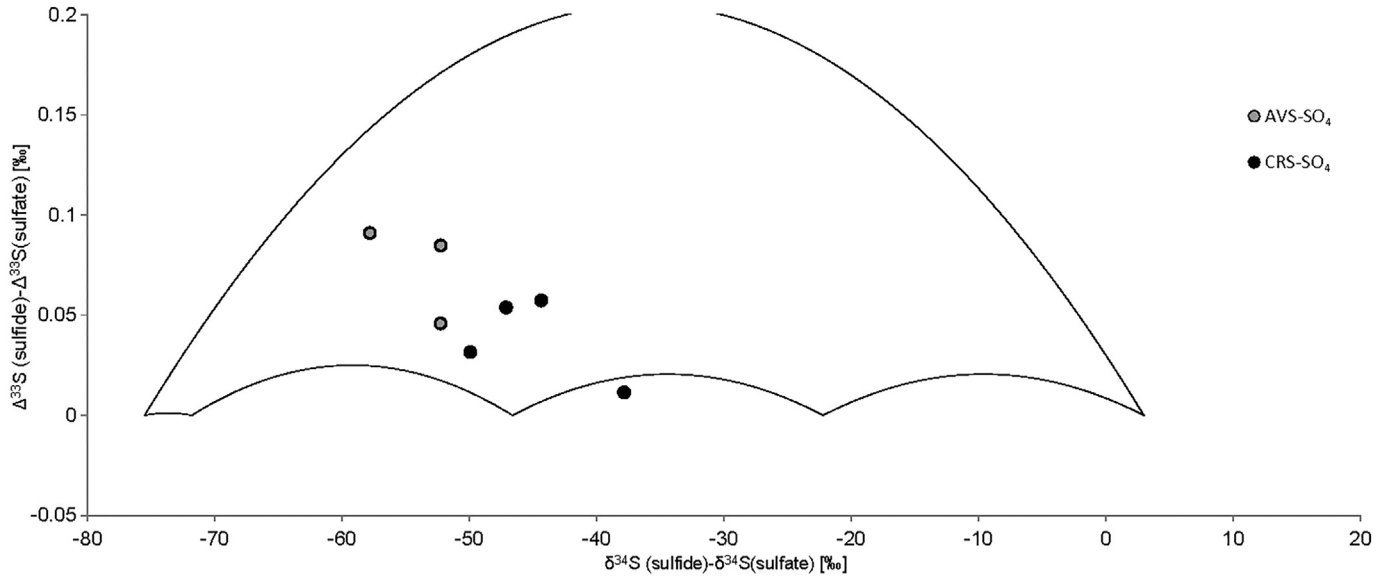

Fig. 9. Offset of $\Delta^{33}S$ vs. offset in $\delta^{34}S$ for reduced sulfur vs. sulfate. Grey circles - AVS-sulfate isotope offset at station AH, black circles - CRS-sulfate isotope offset at station AH. Area inside black lines depicts values for sulfate reduction calculated by Farquhar et al. (2007) for the Brunner and Bernasconi (2005) model.

cycle due to the predominance of ferrous iron rather than sulfide in the pore-water. The dominant control of iron availability on primary composition and early diagenetic signals has previously been described for near-shore environments in the rock record, such as the Late Jurassic Bancs Jumeaux Formation (Tribovillard et al., 2015). The Svalbard sediments studied here can provide important clues on how biogeochemical signatures in such iron-dominated systems are preserved in the sedimentary record.

The variations in sulfur cycling linked to iron in the surface sediments modulate the content and isotope signatures of sulfur compounds. High iron oxide (Fe_{ox1}, Fe_{ox2}) contents, very low S_{org} values, low but detectable CRS contents and persistently light $\delta^{34}S$-CRS values in the sediments at the Van Mijenfjorden and Kongsfjorden stations record the prevailing biogeochemical conditions. These signatures are likely preserved in the sedimentary record. Sulfur (and oxygen) isotopes are more powerful than concentration measurements alone for tracing the addition of new sulfur to existing sulfur phases (e.g. AVS, CRS, organic sulfur) and the identification of specific sulfur transformations (e.g. sulfur disproportionation or oxidation). At sites strongly impacted by glacial runoff, such as the Svalbard fjords, one must take into account the possibility that S_{org} and CRS have a detrital component –this makes detection more challenging, and may lead to misinterpretations. For example, a sulfur isotope offset between AVS and CRS may not be indicative of the presence of two different processes. Although elemental sulfur represents a transient phase in the sedimentary sulfur cycle, it is a powerful indicator of ongoing sulfur cycling. For example, we see clear increases in S^0 for KF-mid2 (and only minor changes in CRS and AVS) and for VMF-out (no change in AVS and CRS concentrations), while the sulfur and oxygen isotopic values of sulfate at these sites remain more elusive.

To elucidate coupled sulfur-metal cycling in the rock record of continental shelf areas that are characterized by very high metal oxide as well as detrital pyrite accumulation rates, a multi-proxy approach is required. This approach should include the analyses of the sulfur (and oxygen) isotope composition of carbonate-associated sulfate (CAS), S_{org} and pyrite, the composition of iron phases (i.e., iron oxides, iron carbonates), combined with the analyses of C/S and C/N ratios. Trace metal signatures represent an additional tool that may, for example, give further insight into iron sources (e.g., via terrigenous input or additional iron shuttling; Anderson and Raiswell, 2004; Lyons and Severmann, 2006; Tribovillard et al., 2015).

6. Summary and conclusions

Our study provides evidence for a prominent role of iron-controlled sulfur cycling in the biogeochemical network of the glacially influenced Svalbard sediments. In the surface sediment of the inner Kongsfjorden and Van Mijenfjorden stations dissimilatory metal reduction plays an important role in organic carbon mineralization; with further distance from the source of glacial iron input, the importance of sulfate reduction likely increases. In all fjords, sulfur is extensively cycled via reductive and oxidative pathways. At the mid- and outer- Kongsfjorden and Van Mijenfjorden stations there is evidence for the occurrence of microbial sulfur disproportionation. At these sites, the input and turnover of highly reducible iron results in a sequence of sulfur transformations in the sediment. The topmost zone shows little sulfur turnover and is neighbored by a zone with sulfate reduction that is matched by equivalent sulfur oxidation to sulfate. This zone is followed by sulfate reduction that is counteracted by sulfur disproportionation, and finally likely a zone with predominant sulfate reduction below. The extent of this zonation is controlled by iron oxide reactivity and accumulation rates, the activity and extent of bioturbation and bioirrigation, and the deposition rate of “fresh” organic carbon.

Careful assessment of the sedimentary iron and sulfur signatures observed in the Svalbard sediments reveals a distinct set of proxy values for Fe oxide, S_{org} and CRS contents that provides a framework for interpreting the Fe-S-C geochemistry of similar iron-rich continental shelf areas in modern environments and for identifying these settings in the rock record.

Supplementary data to this article can be found online at http://dx.doi.org/10.1016/j.chemgeo.2017.06.013.

Acknowledgements

The 2008 sampling campaign was funded by the Max Planck Institute for Marine Microbiology (MPI-MM), Bremen. We would like to thank the captain (S. Henningsen), crew (J. Mortensen) and scientific party for their assistance aboard R/V *Farm*. We also thank the staff of the Kings Bay Marine Laboratory and the AWIPEV Arctic Research Base in Ny Ålesund for their great support. A. Schipper, K. Imhoff and T. Max provided help during lab work at the MPI-MM, Bremen, and O. Dellwig provided support during ICP-OES analyses at IOW Warnemünde. We thank J. Farquhar for support of triple sulfur isotope analyses and G.L. Arnold, T. Lyons, S. Poulton, and S. Severmann for insightful

discussions. We greatly appreciate the constructive comments from S. Bottrell and an anonymous reviewer, and thank the editor J. Fein for his support. Funding for this research to L.M.W. was provided by a DFG research fellowship (We 5015/1-1 and /2-1), funding to A.K. was provided by Marie Curie Outgoing International Fellowship SULFUTOPES number POIF-GA-2008-219586, and to B.B.J. by the Danish National Research Foundation (grant no DNRF104) and ERC Advanced Grant ("MICROENERGY", grant no 294200) under the EU 7th FP.

References

Aharon, P., Fu, B., 2000. Microbial sulfate reduction rates and sulfur and oxygen fractionations at oil and gas seeps in deepwater Gulf of Mexico. Geochim. Cosmochim. Acta 64, 233–246.

Aller, R.C., 1990. Bioturbation and manganese cycling in hemipelagic sediments. Philos. Trans. R. Soc. London, Ser. A 331, 51–68.

Aller, R.C., 1994. The sedimentary Mn cycle in Long Island Sound: Its role as intermediate oxidant and the influence of bioturbation, O_2, and C_{org} flux on diagenetic reaction balances. J. Mar. Res. 52, 259–295.

Aller, R.C., 2014. Sedimentary diagenesis, depositional environments, and benthic fluxes. In: Holland, H.D., Turekian, K.K. (Eds.), Treatise on Geochemistry, Second edition. Elsevier, Oxford, pp. 293–334.

Aller, R.C., Rude, P.D., 1988. Complete oxidation of solid-phase sulfides by manganese and bacteria in anoxic marine sediments. Geochim. Cosmochim. Acta 52, 751–765.

Aller, R.C., Mackin, J.E., Cox, R.T., 1986. Diagenesis of Fe and S in Amazon inner shelf muds: apparent dominance of Fe reduction and implications for the genesis of ironstones. Cont. Shelf Res. 6, 263–289.

Anderson, T.F., Pratt, L.M., 1995. Isotopic Evidence for the Origin of Organic Sulfur and Elemental Sulfur in Marine Sediments, In: Geochemical transformations of sedimentary sulfur. Am. Chem. Soc. 378–396.

Anderson, T.F., Raiswell, R., 2004. Sources and mechansims for the enrichment of highly reactive iron in euxinic Black Sea sediments. Am. J. Sci. 304, 203–233.

Antler, G., Turchyn, A.V., Rennie, V., Herut, B., Sivan, O., 2013. Coupled sulfur and oxygen isotope insight into bacterial sulfate reduction in the natural environment. Geochim. Cosmochim. Acta 118, 98–117.

Arnosti, C., Jørgensen, B.B., 2006. Organic carbon degradation in Arctic marine sediments, Svalbard: a comparison of initial and terminal steps. Geomicrobiol J. 23, 551–563.

Bak, F., Cypionka, H., 1987. A novel type of energy metabolism involving fermentation of inorganic sulfur compounds. Nature 326, 891–892.

Balci, N., Shanks, W., Bernhard, M., Mandernack, K., 2007. Oxygen and sulfur isotope systematics of sulfate produced by bacterial and abiotic oxidation of pyrite. Geochim. Cosmochim. Acta 71, 3796–3811.

Berner, R.A., 1970. Sedimentary pyrite formation. Am. J. Sci. 268, 1–23.

Berner, R.A., 1982. Burial of organic carbon and pyrite sulfur in the modern ocean - its geochemical and environmental significance. Am. J. Sci. 282, 451–473.

Berner, R.A., 1984. Sedimentary pyrite formation - an update. Geochim. Cosmochim. Acta 48, 605–615.

Berner, R.A., 1989. Biogeochemical cycles of carbon and sulfur and their effect on atmospheric oxygen over phanerozoic time. Palaeogeogr. Palaeoclimatol. Palaeoecol. 75, 97–122.

Berner, R.A., Raiswell, R., 1983. Burial of organic carbon and pyrite sulfur in sediments over phanerozoic time - a new theory. Geochim. Cosmochim. Acta 47, 855–862.

Berner, R.A., Westrich, J.T., 1985. Bioturbation and the early diagenesis of carbon and sulfur. Am. J. Sci. 285, 193–206.

Bhatia, M.P., Kujawinski, E.B., Das, S.B., Breier, C.F., Henderson, P.B., Charette, M.A., 2013. Greenland meltwater as a significant and potentially bioavailable source of iron to the ocean. Nat. Geosci. 6, 274–278.

Błaszczyk, M., Jania, J.A., Hagen, J.O., 2009. Tidewater glaciers of Svalbard: recent changes and estimates of calving fluxes. Pol. Polar Res. 30, 85–142.

Böttcher, M.E., Brumsack, H.J., de Lange, G.J., 1998. Sulfate reduction and related stable isotope (34S, 18O) variations in interstitial waters from the eastern Mediterranean. In: Robertson, A.H.F., Emeis, K.-C., Richter, C., Camerlenghi, A. (Eds.), Proc. ODP, Sci. Results. vol. 16. Ocean Drilling Program, College Station, TX, pp. 365–373.

Böttcher, M.E., Bernasconi, S.M., Brumsack, H.J., 1999. Carbon, sulfur, and oxygen isotope geochemistry of interstitial waters from the western Mediterranean. In: Zahn, R., Comas, M.C., Klaus, A. (Eds.), Proceedings of the Ocean Drilling Program, Scientific Results. vol. 161. Ocean Drilling Program, College Station, TX, pp. 413–421.

Böttcher, M.E., Thamdrup, B., Vennemann, T.W., 2001. Oxygen and sulfur isotope fractionation during anaerobic bacterial disproportionation of elemental sulfur. Geochim. Cosmochim. Acta 65, 1601–1609.

Böttcher, M.E., Thamdrup, B., Gehre, M., Theune, A., 2005. 34S/32S and 18O/16O fractionation during sulfur disproportionation by Desulfobulbus propionicus. Geomicrobiol J. 22, 219.

Bottrell, S.H., Newton, R.J., 2006. Reconstruction of changes in global sulfur cycling from marine sulfate isotopes. Earth Sci. Rev. 75, 59–83.

Bottrell, S.H., Mortimer, R.J.G., Davies, I.M., Martyn Harvey, S., Krom, M.D., 2009. Sulphur cycling in organic-rich marine sediments from a Scottish fjord. Sedimentology 56, 1159–1173.

Brabec, M.Y., Lyons, T.W., Mandernack, K.W., 2012. Oxygen and sulfur isotope fractionation during sulfide oxidation by anoxygenic phototrophic bacteria. Geochim. Cosmochim. Acta 83, 234–251.

Brüchert, V., Pratt, L.M., 1996. Contemporaneous early diagenetic formation of organic and inorganic sulfur in estuarine sediments from St. Andrew Bay, Florida, USA. Geochim. Cosmochim. Acta 60, 2325–2332.

Brüchert, V., Knoblauch, C., Jørgensen, B.B., 2001. Controls on stable sulfur isotope fractionation during bacterial sulfate reduction in Arctic sediments. Geochim. Cosmochim. Acta 65, 763–776.

Brunner, B., Bernasconi, S.M., 2005. A revised isotope fractionation model for dissimilatory sulfate reduction in sulfate reducing bacteria. Geochim. Cosmochim. Acta 69, 4759–4771. http://dx.doi.org/10.1016/j.gca.2005.04.015.

Brunner, B., Bernasconi, S.M., Kleikemper, J., Schroth, M.J., 2005. A model for oxygen and sulfur isotope fractionation in sulfate during bacterial sulfate reduction processes. Geochim. Cosmochim. Acta 69, 4773–4785.

Brunner, B., Yu, J.-Y., Mielke, R., MacAskill, J., Madzunkov, S., McGenity, T., Coleman, M., 2008. Different isotope and chemical patterns of pyrite oxidation related to lag and exponential growth phases of Acidithiobacillus ferrooxidans reveal a microbial growth strategy. Earth Planet. Sci. Lett. 270, 63–72.

Brunner, B., Einsiedl, F., Arnold, G.L., Müller, I., Templer, S., Bernasconi, S., 2012. The reversibility of dissimilatory sulphate reduction and the cell-internal multistep reduction of sulphite to sulphide: insights from the oxygen isotope composition of sulphate. Isot. Environ. Health Stud. 48, 33–54.

Brunner, B., Arnold, G.L., Røy, H., Müller, I.A., Jørgensen, B.B., 2016. Off limits: sulfate below the sulfate-methane transition. Front. Earth Sci. http://dx.doi.org/10.3389/feart.2016.00075.

Butler, I.B., Rickard, D., 2000. Framboidal pyrite formation via the oxidation of iron (II) monosulfide by hydrogen sulphide. Geochim. Cosmochim. Acta 64, 2665–2672.

Butler, I.B., Böttcher, M.E., Rickard, D., Oldroyd, A., 2004. Sulfur isotope partitioning during experimental formation of pyrite via the polysulfide and hydrogen sulfide pathways: implications for the interpretation of sedimentary and hydrothermal pyrite isotope records. Earth Planet. Sci. Lett. 228, 495–509.

Calvert, S.E., Pedersen, T.F., 1993. Geochemistry of recent oxic and anoxic marine sediments: implications for the geological record. Mar. Geol. 113, 67–88.

Canfield, D.E., 1989. Reactive iron in marine sediments. Geochim. Cosmochim. Acta 53, 619–632.

Canfield, D.E., 2001. Isotope fractionation by natural populations of sulfate-reducing bacteria. Geochim. Cosmochim. Acta 65, 1117–1124.

Canfield, D.E., Thamdrup, B., 1994. The production of 34S–depleted sulfide during bacterial disproportionation of elemental Sulphur. Science 266, 1973–1975.

Canfield, D.E., Thamdrup, B., 1996. Fate of elemental sulfur in an intertidal sediment. FEMS Microbiol. Ecol. 19, 95–103.

Canfield, D.E., Jorgensen, B.B., Fossing, H., Glud, R., Gundersen, J., Ramsing, N.B., Thamdrup, B., Hansen, J.W., Nielsen, L.P., Hall, P.O.J., 1993. Pathways of organic carbon oxidation in three continental margin sediments. Mar. Geol. 113, 27–40.

Canfield, D.E., Stewart, F.J., Thamdrup, B., De Brabandere, L., Dalsgaard, T., Delong, E.F., Revsbach, N.P., Ulloa, O., 2010a. A cryptic sulfur cycle in oxygen-minimum-zones waters off the Chilean coast. Science 33 (6009), 1375–1378.

Canfield, D.E., Farquhar, J., Zerkle, A.L., 2010b. High isotope fractionations during sulfate reduction in a low-sulfate euxinic ocean analog. Geology 38, 415–418. http://dx.doi.org/10.1130/G30723.1.

Canion, A., Overholt, W.A., Kostka, J.E., Huettel, M., Lavik, G., Kuypers, M.M.M., 2014. Temperature response of denitrification and anaerobic ammonium oxidation rates and microbial community structure in Arctic fjord sediments. Environ. Microbiol. 16 (10), 3331–3344.

Cline, J., 1969. Spectrophotometric determination of hydrogen sulfide in natural waters. Limnol. Oceanogr. 14, 454–458.

Cottier, F., Tverberg, V., Inall, M., Svendsen, H., Nilsen, F., Griffiths, C., 2005. Water mass modification in an Arctic fjord through cross-shelf exchange: the seasonal hydrography of Kongsfjorden, Svalbard. J. Geophys. Res. Oceans 110, C12.

Dallmann, W.K. (Ed.), 1999. Lithostratigraphic Lexicon of Svalbard. Norsk Polarinstitutt, Tromsø, pp. 215–263.

Dallmann, W.K., Ohta, Y., Elvevold, S., Blomeier, D., 2002. Bedrock map of Svalbard and Jan Mayen. In: Norsk Polarinstitutt Temakart No. 33. Norsk Polarinstitutt, Oslo.

Eilertsen, H.C., Taasen, J.P., Weslawski, J.M., 1989. Phytoplankton studies in the fjords of West Spitsbergen: physical environment and production in spring and summer. J. Plankton Res. 11 (6), 1245–1260.

Farquhar, J., Johnston, D.T., Wing, B.A., 2007. Implications of conservation of mass effects on mass-dependent isotope fractionations: influence of network structure on sulfur isotope phase space of dissimilatory sulfate reduction. Geochim. Cosmochim. Acta 71, 5862–5875.

Farquhar, J., Canfield, D.E., Masterson, A., Bao, H., Johnston, D., 2008. Sulfur and oxygen isotope study of sulfate reduction in experiments with natural populations from Faellestrand, Denmark. Geochim. Cosmochim. Acta 72, 2805–2821.

Ferdelman, T.G., Lee, C., Pantoja, S., Harder, J., Bebout, B.M., Fossing, H., 1997. Sulfate reduction and methanogenesis in a Thioploca-dominated sediment off the coast of Chile. Geochim. Cosmochim. Acta 61, 3065–3079.

Finster, K., Liesack, W., Thamdrup, B., 1998. Elemental sulfur and thiosulfate disproportionation by Desulfocapsa sulfoexigens sp nov, a new anaerobic bacterium isolated from marine surface sediment. Appl. Environ. Microbiol. 64, 119–125.

Fossing, H., Jørgensen, B.B., 1989. Measurement of bacterial sulfate reduction in sediments - evaluation of a single-step chromium reduction method. Biogeochemistry 8, 205–222.

Fritz, P., Basharmal, G.M., Drimmie, R.J., Ibsen, J., Qureshi, R.M., 1989. Oxygen isotope exchange between sulfate and water during bacterial reduction of sulfate. Chem. Geol. 79, 99–105.

Froelich, P.N., Klinkhammer, G.P., Bender, M.L., Luedtke, N.A., Heath, G.R., Cullen, D., Dauphin, P., Hammond, D., Hartman, B., Maynard, V., 1979. Early oxidation of

organic matter in pelagic sediments of the eastern equatorial Atlantic: suboxic diagenesis. Geochim. Cosmochim. Acta 43, 1075–1090.
Fry, B., Gest, H., Hayes, J.M., 1984. Isotope effects associated with the anaerobic oxidation of sulfide by the purple photosynthetic bacterium, Chromatium vinosum. FEMS Microbiol. Lett. 22, 283–287.
Fry, B., Gest, H., Hayes, J.M., 1985. Isotope effects associated with the anaerobic oxidation of sulfite and thiosulfate by the photosynthetic bacterium, Chromatium vinosum. FEMS Microbiol. Lett. 27, 227–232.
Fry, B., Ruf, W., Gest, H., Hayes, J.M., 1988. Sulfur isotope effects associated with oxidation of sulfide by O2 in aqueous solution. Chem. Geol. 73, 205–210.
Fuseler, K., Cypionka, H., 1995. Elemental sulfur as an intermediate of sulfide oxidation with oxygen by Desulfobulbus propionicus. Arch. Microbiol. 164 (2), 104–109.
Glasser, N.F., Hambrey, M.J., 2001. Styles of sedimentation beneath Svalbard valley glaciers under changing dynamic and thermal regimes. J. Geol. Soc. 158, 697–707.
Gröger, J., Franke, J., Hamer, K., Schulz, H.D., 2009. Quantitative recovery of elemental sulfur and improved selectivity in a chromium-reducible sulfur distillation. Geostand. Geoanal. Res. 33 (1), 17–27.
Habicht, K.S., Canfield, D.E., 2001. Isotope fractionation by sulfate-reducing natural populations and the isotope composition of sulfide in marine sediments. Geology 29, 555–558.
Hagen, J.O., Lefauconnier, B., 1995. Reconstructed runoff from the high Arctic Basin Bayelva based on mass-balance measurements. Hydrol. Res. 26, 285–296.
Hagen, J.O., Liestøl, O., Roland, E., Jørgensen, T., 1993. Glacier atlas of Svalbard and Jan Mayen. In: Norsk Polarinstitutt Meddelser 129.
Hald, M., Korsun, S., 2008. The 8200 cal. yr BP event reflected in the Arctic fjord, Van Mijenfjorden, Svalbard. The Holocene 18, 981–990.
Hald, M., Dahlgren, T., Olsen, T.-E., Lebesbye, E., 2001. Late Holocene paleoceanography in Van Mijenfjorden, Svalbard. Polar Res. 20, 23–35.
Harland, W.B., 1997. The geology of Svalbard. Geol. Soc. Lond. Mem. 17 (521 pp.).
Hartgers, W.A., Lopez, J.F., Sinninghe Damste, J.S., Reiss, C., Maxwell, J.R., Grimalt, J.O., 1997. Sulfur-binding in recent environments. II. Speciation of sulfur and iron and implications for the occurrence of organo-sulfur compounds. Geochim. Cosmochim. Acta 61, 4769–4788.
Hawkings, J.R., Wadham, J.L., Tranter, M., Raiswell, R., Benning, L.G., Statham, P.J., Tedstone, A., Nienow, P., Lee, K., Telling, J., 2014. Ice sheets as a significant source of highly reactive nanoparticulate iron to the oceans. Nat. Commun. 5, 3239.
Hebbeln, D., Berner, H., 1993. Surface sediment distribution in the Fram Strait. Deep-Sea Res. I 40, 1731–1745.
Hegseth, E.N., Tverberg, V., 2013. Effect of Atlantic water inflow on timing of the phytoplankton spring bloom in a high Arctic fjord (Kongsfjorden, Svalbard). J. Mar. Syst. 113-114, 94–105.
Hensen, C., Zabel, M., Pfeifer, K., Schwenk, T., Kasten, S., Riedinger, N., Schulz, H.D., Boetius, A., 2003. Control of sulfate pore-water profiles by sedimentary events and the significance of anaerobic oxidation of methane for the burial of sulfur in marine sediments. Geochim. Cosmochim. Acta 67, 2631–2647.
Hjelle, A., 1993. The geology of Svalbard: Oslo. In: Polarhåndbok No. 6. Norsk Polarinstitutt, pp. 163.
Hodal, H., Falk-Petersen, S., Hop, H., Kristiansen, S., Reigstad, M., 2012. Spring bloom dynamics in Kongsfjorden, Svalbard: nutrients, phytoplankton, protozoans and primary production. Polar Biol. 35, 191–203.
Hodgkins, R., 1997. Glacier hydrology in Svalbard, Norwegian high Arctic. Quat. Sci. Rev. 16, 957–973.
Hodgkins, R., Cooper, R., Wadham, J., Tranter, M., 2003. Suspended sediment fluxes in a high-Arctic glacierised catchment: implications for fluvial sediment storage. Sediment. Geol. 162, 105–117.
Hodgkins, R., Cooper, R., Wadham, J., Tranter, M., 2009. The hydrology of the proglacial zone of a high-Arctic glacier (Finsterwalderbreen, Svalbard): atmospheric and surface water fluxes. J. Hydrol. 378, 150–160.
Hodson, A., Nowak, A., Christiansen, H., 2016. Glacial and periglacial floodplain sediments regulate hydrologic transfer of reactive iron to a high arctic fjord. Hydrol. Process. 30, 1219–1229.
Hoehler, T.M., Alperin, M.J., Albert, D.B., Martens, C.S., 1994. Field and laboratory studies of methane oxidation in an anoxic marine sediment: evidence for a methanogen-sulfate reducer consortium. Glob. Biogeochem. Cycles 8, 451–463.
Holmkvist, L., Ferdelman, T.G., Jørgensen, B.B., 2011. A cryptic sulfur cycle driven by iron in the methane zone of marine sediment (Aarhus Bay, Denmark). Geochim. Cosmochim. Acta 75, 3581–3599.
Hop, H., Pearson, T., Hegseth, E.N., Kovacs, K.M., Wiencke, C., Kwasniewski, S., Eiane, K., Mehlum, F., Gulliksen, B., Wlodarska-Kowalezuk, M., Lydersen, C., Weslawski, J.M., Cochrane, S., Gabrielsen, G.W., Leakey, R.J.G., Lonne, O.J., Zajaczkowski, M., Falk-Petersen, S., Kendall, M., Wangberg, S.A., Bischof, K., Voronkov, A.Y., Kovaltchouk, N.A., Wiktor, J., Poltermann, M., di Prisco, G., Papucci, C., Gerland, S., 2002. The marine ecosystem of Kongsfjorden, Svalbard. Polar Res. 21, 167–208.
Howe, J.A., Moreton, S.G., Morri, C., Morris, P., 2003. Multibeam bathymetry and the depositional environments of Kongsfjorden and Krossfjorden, western Spitsbergen, Svalbard. Polar Res. 22, 301–316.
Hubert, C., Voordouw, G., Mayer, B., 2009. Elucidating microbial processes in nitrate- and sulfate reducing systems using sulfur and oxygen isotope ratios: the example of oil reservoir souring control. Geochim. Cosmochim. Acta 73, 3864–3879.
Hyacinthe, C., Van Cappellen, P., 2004. An authigenic iron phosphate phase in estuarine sediments: composition, formation and chemical reactivity. Mar. Chem. 91, 227–251.
Johnston, D.T., Farquhar, J., Wing, B.A., Kaufman, A., Canfield, D.E., Habicht, K.S., 2005. Multiple sulfur isotope fractionations in biological systems: a case study with sulfate reducers and sulfur disproportionators. Am. J. Sci. 305, 645–660.
Jørgensen, B.B., 1982. Mineralization of organic matter in the sea bed - the role of sulphate reduction. Nature 296, 643–645.
Jørgensen, B.B., 1990. A thiosulfate shunt in the sulfur cycle of marine sediments. Science 249, 152–154.
Jørgensen, B.B., Bak, F., 1991. Pathways and microbiology of thiosulfate transformations and sulfate reduction in a marine sediment (Kattegat, Denmark). Appl. Environ. Microbiol. 57, 847–856.
Jørgensen, B.B., Kasten, S., 2006. Sulfur cycling and methane oxidation. In: Schulz, H.D., Zabel, M. (Eds.), Marine Geochemistry. Springer-Verlag, Heidelberg, pp. 574.
Jørgensen, B.B., Nelson, D.C., 2004. Sulfide oxidation in marine sediments: geochemistry meets microbiology. In: Amend, J.P., Edwards, K.J., Lyons, T.W. (Eds.), Sulfur Biogeochemistry – Past and Present. Geological Society of America, pp. 36–81.
Kamyshny Jr., A., 2009. Solubility of cyclooctasulfur in pure water and sea water at different temperatures. Geochim. Cosmochim. Acta 73, 6022–6028.
Kanneworff, E., Nicolaisen, W., 1983. A simple, hand-operated quantitative bottom sampler. Ophelia 22, 253–255.
Kaplan, I.R., Rittenberg, S.C., 1964. Microbiological fractionation of sulphur isotopes. J. Gen. Microbiol. 34, 195–212.
Kelly, D.P., 2008. Stable sulfur isotope fractionation by the green bacterium Chlorobaculum Parvum during photolithoautotrophic growth on sulfide. Pol. J. Microbiol. 57 (4), 275–279.
Kelly, D., Shergill, J., Lu, W.-P., Wood, A., 1997. Oxidative metabolism of inorganic sulfur compounds by bacteria. Antonie Van Leeuwenhoek 71, 95–107.
Kim, J.-H., Peterse, F., Willmott, V., Klitgaard Kristensen, D., Baas, M., Schouten, S., Sinninghe Damsté, J.S., 2011. Large ancient organic matter contributions to Arctic marine sediments (Svalbard). Limnol. Oceanogr. 56, 1463–1474.
Kohnen, M., Damste, J.S., ten Haven, H.L., De Leeuw, J.W., 1989. Early incorporation of polysulfides in sedimentary organic matter. Nature 341, 640–641.
Kostka, J.E., Luther III, G.W., 1994. Partitioning and speciation of solid phase iron in saltmarsh sediments. Geochim. Cosmochim. Acta 58, 1701–1710.
König, M., Nuth, C., Kohler, J., Moholdt, G., Pettersen, R., 2014. A digital glacier database for svalbard. In: Kargel, S.J., Leonard, J.G., Bishop, P.M., Kääb, A., Raup, H.B. (Eds.), Global Land Ice Measurements from Space. Springer Berlin Heidelberg, Berlin, Heidelberg, pp. 229–239.
Kostka, J.E., Thamdrup, B., Glud, R.N., Canfield, D.E., 1999. Rates and pathways of carbon oxidation in permanently cold Arctic sediments. Mar. Ecol. Prog. Ser. 180, 7–21.
Koziorowska, K., Kuliński, K., Pempkowiak, J., 2016. Sedimentary organic matter in two Spitsbergen fjords: terrestrial and marine contributions based on carbon and nitrogen contents and stable isotopes composition. Cont. Shelf Res. 113, 38–46.
Krämer, M., Cypionka, H., 1989. Sulfate formation via ATP sulfurylase in thiosulfate- and sulfite-disproportionating bacteria. Arch. Microbiol. 151, 232–237.
Kuliński, K., Kędra, M., Legeżyńska, J., Gluchowska, M., Zaborska, A., 2014. Particulate organic matter sinks and sources in high Arctic fjord. J. Mar. Syst. 139, 27–37.
Lord III, C.J., 1980. The chemistry and cycling of iron, manganese and sulfur in salt marsh sediment. PhD thesis University of Delaware 177 pp.
Lovley, D.R., Phillips, E.J.P., 1994. Novel processes of anaerobic sulfate production from elemental sulfur by sulfate-reducing bacteria. Appl. Environ. Microbiol. 60 (6), 2394–2399.
Luther, G.W., 1987. Pyrite oxidation and reduction: molecular orbital theory considerations. Geochim. Cosmochim. Acta 51, 3193–3199.
Luther III, G.W., 1991. Pyrite synthesis via polysulfide compounds. Geochim. Cosmochim. Acta 55, 2839–2849.
Luther III, G.W., Church, T.M., 1988. Seasonal cycling of sulfur and iron in porewaters of a Delaware salt marsh. Mar. Chem. 23 (3-4), 295–309.
Luther III, G.W., Rickard, D.T., 2005. Metal sulfide cluster complexes and their biogeochemical importance in the environment. J. Nanopart. Res. 7 (4), 389–407.
Lyons, T.W., Severmann, S., 2006. A critical look at iron paleoredox proxies based on new insights from modern euxinic marine basins. Geochim. Cosmochim. Acta 70, 5698–5722.
Mandernack, K.W., Krouse, H.R., Skei, J.M., 2003. A stable sulfur and oxygen isotopic investigation of sulfur cycling in an anoxic marine basin, Framvaren Fjord, Norway. Chem. Geol. 195, 181–200.
Manley, T.O., 1995. Branching of Atlantic water within the Greenland-Spitsbergen passage - an estimate of recirculation. J. Geophys. Res. Oceans 100, 20627–20634.
Mehra, O.P., Jackson, M.L., 1960. Iron oxide removal from soils and clays by a dithionite-citrate system buffered with sodium bicarbonate. In: Proc. 7th nat. Conf. Clays, pp. 317–327.
Meyers, P.A., 1994. Preservation of elemental and isotopic source identification of sedimentary organic matter. Chem. Geol. 114, 289–302.
Mieschner, D., Rumohr, J., 1974. A light-weight, high-momentum gravity corer for subaqueous sediments. Senckenberg. Marit. 6, 105–117.
Mizutani, Y., Rafter, T.A., 1973. Isotopic behavior of sulphate oxygen in the bacterial reduction of sulphate. Geochem. J. 6, 183–191.
Morse, J.W., 1991. Oxidation-kinetics of sedimentary pyrite in seawater. Geochim. Cosmochim. Acta 55, 3665–3667.
Mortimer, R.J.G., Galsworthy, A.M.J., Bottrell, S.H., Wilmot, L.E., Newton, R.J., 2001. Experimental evidence for rapid biotic and abiotic reduction of Fe (III) at low temperatures in salt marsh sediments: a possible mechanism for formation of modern sedimentary siderite concretions. Sedimentology 58, 1514–1529.
Moses, C.O., Herman, J.S., 1991. Pyrite oxidation at circumneutral pH. Geochim. Cosmochim. Acta 55, 471–482.
Nickel, M., Vandieken, V., Brüchert, V., Jørgensen, B.B., 2008. Microbial Mn(IV) and Fe (III) reduction in northern Barents Sea sediments under different conditions of ice cover and organic carbon deposition. Deep-Sea Res. II Top. Stud. Oceanogr. 55, 2390–2398.
Nilsen, F., Cottier, F., Skogseth, R., Mattsson, S., 2008. Fjord–shelf exchanges controlled by ice and brine production: the interannual variation of Atlantic water in Isfjorden,

Svalbard. Cont. Shelf Res. 28, 1838–1853.
Ohta Y., Hjelle A. and Dallmann W.K. (2007) Geological map Svalbard 1:100 000, sheet A4G, Vasahalvoya. Norsk Polarinstitutt Temakart No. 40.
Ohta Y., Hjelle A. and Dallmann W. K. (2008) Geological map Svalbard 1:100 000, sheet A5G, Magdalenefjorden. Norsk Polarinstitutt Temakart No. 41.
Popova, E.E., Yool, A., Coward, A.C., Aksenov, Y.K., Alderson, S.G., de Cuevas, B.A., Anderson, T.R., 2010. Control of primary production in the Arctic by nutrients and light: insights from a high resolution ocean general circulation model. Biogeosciences 7, 3569–3591.
Poser, A., Vogt, C., Knöller, K., Ahlheim, J., Weiss, H., Kleinsteuber, S., Richnow, H.-H., 2014. Stable sulfur and oxygen isotope fractionation of anoxic sulfide oxidation by two different enzymatic pathways. Environ. Sci. Technol. 48, 9094–9102.
Poulton, S.W., Canfield, D.E., 2005. Development of a sequential extraction procedure for iron: implications for iron partitioning in continentally derived particulates. Chem. Geol. 214, 209–221.
Raiswell, R., Tranter, M., Benning, L.G., Siegert, M., De'ath, R., Huybrechts, P., Payne, T., 2006. Contributions from glacially derived sediment to the global iron (oxyhydr) oxide cycle: implications for iron delivery to the oceans. Geochim. Cosmochim. Acta 70, 2765–2780.
Raiswell, R., Benning, L.G., Tranter, M., Tulaczyk, S., 2008. Bioavailable iron in the Southern Ocean: the significance of the iceberg conveyor belt. Geochem. Trans. 9, 1–9.
Raiswell, R., Vu, H.P., Brinza, L., Benning, L.G., 2010. The determination of labile Fe in ferrihydrite by ascorbic acid extraction: methodology, dissolution kinetics and loss of solubility with age and de-watering. Chem. Geol. 278, 70–79.
Reeburgh, W.S., 1983. Rates of biogeochemical processes in anoxic sediments. Annu. Rev. Earth Planet. Sci. 11, 269–298.
Rees, C.E., 1973. Steady-state model for sulfur isotope fractionation in bacterial reduction processes. Geochim. Cosmochim. Acta 37, 1141–1162.
Rickard, D., Luther III, G.W., 1997. Kinetics of pyrite formation by the H2S oxidation of iron (II) monosulfide in aqueous solutions between 25 and 125°C: the mechanism. Geochim. Cosmochim. Acta 61, 135–147.
Riedinger, N., Brunner, B., Krastel, S., Arnold, G.L., Wehrmann, L.M., Formolo, M.J., Beck, A., Bates, S.M., Henkel, S., Kasten, S., Lyons, T.W., 2017. Sulfur cycling in an iron oxide-dominated, dynamic marine depositional system: the argentine continental margin. Front. Earth Sci. 5, 33. http://dx.doi.org/10.3389/feart.2017.00033.
Rippin, D., Willis, I., Arnold, N., Hodson, A., Moore, J., Kohler, J., Bjornsson, H., 2003. Changes in geometry and subglacial drainage of Midre Lovenbreen, Svalbard, determined from digital elevation models. Earth Surf. Process. Landf. 28, 273–298.
Robador, A., Brüchert, V., Jørgensen, B.B., 2009. The impact of temperature change on the activity and community composition of sulfate-reducing bacteria in arctic versus temperate marine sediments. Environ. Microbiol. 11, 1692–1703.
Rudnicki, M.D., Elderfield, H., Spiro, B., 2001. Fractionation of sulfur isotopes during bacterial sulfate reduction in deep ocean sediments at elevated temperatures. Geochim. Cosmochim. Acta 65, 777–789.
Schippers, A., 2004. Biogeochemistry of metal sulfide oxidation in mining environments, sediments, and soils. Geol. Soc. Am. Spec. Pap. 379, 49–62.
Schippers, A., Jørgensen, B.B., 2001. Oxidation of pyrite and iron sulfide by manganese dioxide in marine sediments. Geochim. Cosmochim. Acta 65, 915–922.
Schippers, A., Jørgensen, B.B., 2002. Biogeochemistry of pyrite and iron sulfide oxidation in marine sediments. Geochim. Cosmochim. Acta 66, 85–92.
Schoonen, M.A.A., 2004. Mechanisms of sedimentary pyrite formation. In: Amend, J.P., Edwards, K.J., Lyons, T.W. (Eds.), Sulfur Biogeochemistry - Past and Present, 379 ed. pp. 117–134.
Schoonen, M.A.A., Barnes, H.L., 1991. Reactions forming pyrite and marcasite from solution: II. Via FeS precursors below 100°C. Geochim. Cosmochim. Acta 55, 1505–1514.
Sim, M.S., Bosak, T., Ono, S., 2011. Large sulfur isotope fractionation does not require disproportionation. Science 333, 74–77.
Sinninghe Damste, J.S., De Leeuw, J.W., 1990. Analysis, structure and geochemical significance of organically-bound sulphur in the geosphere: state of the art and future research. Org. Geochem. 16, 1077–1101.
Sinninghe Damste, J.S., Eglinton, T.I., de Leeuw, J.W., Schenck, P.A., 1989. Organic sulphur in macromolecular sedimentary organic matter. I. Structure and origin of sulphur-containingmoieties in kerogen, asphaltenes and coal as revealed by flash pyrolysis. Geochim. Cosmochim. Acta 53, 873–889.
Ślubowska-Woldengen, M., Rasmussen, T.L., Koç, N., Klitgaard-Kristensen, D., Nilsen, F., Solheim, A., 2007. Advection of Atlantic water to the western and northern Svalbard shelf since 17,500 cal yr BP. Quat. Sci. Rev. 26, 463–478.
Statham, P.J., Skidmore, M., Tranter, M., 2008. Inputs of glacially derived dissolved and colloidal iron to the coastal ocean and implications for primary productivity. Glob. Biogeochem. Cycles 22 (3). http://dx.doi.org/10.1029/2007GB003106.
Steel, R.J., Worsley, D., 1984. Svalbard's post-Caledonian strata - an atlas of sedimentational patterns and palaeogeographic evolution. In: Spencer, A.M. (Ed.), Petroleum Geology of the North European Margin. Graham & Trotman, Norwegian Petroleum Society, pp. 109–135.
Svendsen, H., Beszczynska-Moller, A., Hagen, J.O., Lefauconnier, B., Tverberg, V., Gerland, S., Orbaek, J.B., Bischof, K., Papucci, C., Zajaczkowski, M., Azzolini, R., Bruland, O., Wiencke, C., Winther, J.G., Dallmann, W., 2002. The physical environment of Kongsfjorden-Krossfjorden, an Arctic fjord system in Svalbard. Polar Res. 21, 133–166.
Thamdrup, B., Finster, K., Hansen, W., Bak, F., 1993. Bacterial disproportionation of elemental sulfur coupled to chemical reduction of iron and manganese. Appl. Environ. Microbiol. 59, 101–108.
Thamdrup, B., Fossing, H., Jørgensen, B.B., 1994. Manganese, iron and sulfur cycling in a coastal marine sediment, Aarhus bay, Denmark. Geochim. Cosmochim. Acta 58, 5115–5129.
Thurston, R.S., Mandernack, K.W., Shanks III, W.C., 2010. Laboratory chalcopyrite oxidation by Acidithiobacillus ferrooxidans: oxygen and sulfur isotope fractionation. Chem. Geol. 269, 252–261.
Toran, L., Harris, R.F., 1989. Interpretation of sulfur and oxygen isotopes in biological and abiological sulfide oxidation. Geochim. Cosmochim. Acta 53, 2341–2348.
Tribovillard, N., Hatem, E., Averbach, O., Barbecot, F., Bout-Roumazeilles, V., Trentesaux, A., 2015. Iron availability as a dominant control on the primary composition and diagenetic overprint of organic-matter-rich rocks. Chem. Geol. 401, 67–82.
Vairavamurthy, A., Mopper, K., 1987. Geochemical formation of organic sulphur compounds (thiols) by addition of H_2S to sedimentary organic matter. Nature 329, 623–625.
Vairavamurthy, M.A., Orr, W.L., Manowitz, B., 1995. Geochemical transformations of sedimentary sulfur: an introduction, geochemical transformations of sedimentary sulfur. Am. Chem. Soc. 1–14.
Valentine, D.L., Reeburgh, W.S., 2000. New perspectives on anaerobic methane oxidation. Environ. Microbiol. 2, 477–484.
Vandieken, V., Finke, N., Jørgensen, B.B., 2006a. Pathways of carbon oxidation in an Arctic fjord sediment (Svalbard) and isolation of psychrophilic and psychrotolerant Fe(III)-reducing bacteria. Mar. Ecol. Prog. Ser. 322, 29–41.
Vandieken, V., Nickel, M., Jørgensen, B.B., 2006b. Carbon mineralization in Arctic sediments northeast of Svalbard: Mn(IV) and Fe(III) reduction as principal anaerobic respiratory pathways. Mar. Ecol. Prog. Ser. 322, 15–27.
Velle, H.J., 2012. Holocene sedimentary environments in Smeerenburgfjorden, Spitsbergen. (Master Thesis) University of Trømso.
Wadham, J.L., Bottrell, S., Tranter, M., Raiswell, R., 2004. Stable isotope evidence for microbial sulphate reduction at the bed of a polythermal high Arctic glacier. Earth Planet. Sci. Lett. 219, 341–355.
Wadham, J.L., Cooper, R.J., Tranter, M., Bottrell, S., 2007. Evidence for widespread anoxia in the proglacial zone of an Arctic glacier. Chem. Geol. 243, 1–15.
Wadham, J.L., De'ath, R., Monteiro, F.M., Tranter, M., Ridgwell, A., Raiswell, R., Tulaczyk, S., 2013. The potential role of the Antarctic ice sheet in global biogeochemical cycles. Earth Environ. Sci. Trans. R. Soc. Edinb. 104, 55–67.
Wagner, T., Dupont, L., 1999. Terrestrial organic matter in marine sediments: analytical approaches and eolian-marine records of the central equatorial Atlantic. In: Fischer, G., Wefer, G. (Eds.), The Use of Proxies in Paleoceanography: Examples from the South Atlantic. Springer, New York, pp. 547–574.
Wehrmann, L.M., Formolo, M.J., Owens, J.D., Raiswell, R., Ferdelman, T.G., Riedinger, N., Lyons, T.W., 2014. Iron and manganese speciation and cycling in glacially influenced high-latitude fjord sediments (West Spitsbergen, Svalbard): evidence for a benthic recycling-transport mechanism. Geochim. Cosmochim. Acta 141, 628–655.
Wehrmann, L.M., Titschack, J., Böttcher, M.E., Ferdelman, T.G., 2015. Linking sedimentary sulfur and iron biogeochemistry to growth patterns of a cold-water coral mound in the Porcupine Basin, S.W. Ireland (IODP expedition 307). Geobiology 13, 424–442.
Werne, J.P., Hollander, D.J., Behrens, A., Schaeffer, P., Albrecht, P., Sinninghe Damsté, J.S.S., 2000. Timing of early diagenetic sulfurization of organic matter: a precursor–product relationship in Holocene sediments of the anoxic Cariaco Basin, Venezuela. Geochim. Cosmochim. Acta 64, 1741–1751.
Werne, J.P., Lyons, T.W., Hollander, D.J., Formolo, M.J., Sinninghe Damsté, J.S., 2003. Reduced sulfur in euxinic sediments of the Cariaco Basin: sulfur isotope constraints on organic sulfur formation. Chem. Geol. 195, 159–179.
Werne, J.P., Hollander, D.J., Lyons, T.W., Sinninghe Damsté, J.S., 2004. Organic sulfur biogeochemistry: recent advances and future research directions. Geol. Soc. Am. Spec. Pap. 379, 135–150.
Werne, J.P., Lyons, T.W., Hollander, D.J., Schouten, S., Hopmans, E.C., Sinninghe Damsté, J.S., 2008. Investigating pathways of diagenetic organic matter sulfurization using compound-specific sulfur isotope analysis. Geochim. Cosmochim. Acta 72, 3489–3502.
Wiktor, J., 1999. Early spring microplankton development under fast ice covered fjords of Svalbard, Arctic. Oceanologia 41 (1), 51–72.
Wilkin, R.T., Barnes, H.L., 1996. Pyrite formation by reactions of iron monosulfides with dissolved inorganic and organic sulfur species. Geochim. Cosmochim. Acta 60, 4167–4179.
Wing, B.A., Halevy, I., 2014. Intracellular metabolite levels shape sulfur isotope fractionation during microbial sulfate respiration. Proc. Natl. Acad. Sci. 111, 18116–18125.
Wortmann, U.G., Bernasconi, S.M., Bottcher, M.E., 2001. Hypersulfidic deep biosphere indicates extreme sulfur isotope fractionation during single-step microbial sulfate reduction. Geology 29, 647–650.
Zaborska, A., Wlodarska-Kowalczuk, M., Legeżyńska, J., Jankowska, E., Winogradow, A., Deja, K., 2017. Sedimentary organic matter sources, benthic consumption and burial in west Spitsbergen fjords – signs of maturing of Arctic fjordic systems? J. Mar. Syst (in press).
Zerkle, A.L., Farquar, J., Johnston, D.T., Cox, R.P., Canfield, D., 2009. Fractionation of multiple sulfur isotopes during phototrophic oxidation of sulfide and elemental sulfur by a green sulfur bacterium. Geochim. Cosmochim. Acta 73, 291–306.
Zerkle, A.L., Kamyshny Jr., A., Kump, L.R., Farquhar, J., Oduro, H., Arthur, M.A., 2010. Sulfur cycling in a stratified euxinic lake with moderately high sulfate: constraints from quadruple S isotopes. Geochim. Cosmochim. Acta 74, 4953–4970.
Zopfi, J., Ferdelman, T., Fossing, H., 2004. Distribution and fate of sulfur intermediates—sulfite, tetrathionate, thiosulfate, and elemental sulfur—in marine sediments. Geol. Soc. Am. Spec. Pap. 379, 97–116.